

## CHAPTER 2

---

## **CHAPTER 2**

# **NOISE FEATURE ANALYSIS OF MOS GAS SENSORS**

---

### **2.0 Introduction:**

Electronic nose uses an array of gas sensors with different selectivities towards the various classes of compounds, and the composite signal of the array is used in conjunction with chemometrics for the classification and identification of classes of the samples. There exist several materials to build gas sensors as discussed in **Chapter 1**.

MOS gas sensors are one of the most widely spread devices used for E-Nose applications due to their low cost, acceptable response, low recovery times and robustness. Electronic noses are more widely used in environmental monitoring, food quality detection and medicine. The odour recognition process in electronic nose begins in the sensor system which is responsible for capturing or measurement of the odourant stimulus through the sensitivity of its sensors. Each odourant is presented to the sensor system, which generates a pattern of resistance values that characterize the odour. This pattern is presented to the recognition system, which in turn classifies the odour.

The preprocessing of the data is done before the classification of odour. The data preprocessing is important because a number of different problems can compromise the performance of the sensor system which are as follows:

- i) The odour signal can present disturbance or noise,
- ii) The data acquisition may be unstable,
- iii) The signal propagation through the communication channel between the sensor and pattern recognition systems can be contaminated by the interference signals from the environment.

The odour responses must be analyzed before the pattern recognition process to compensate for the concentration drifts in the response arrays, eliminate noise and normalize data.

Noise in gas sensors is considered to be any unwanted effect that obscures the measurement of the desired signal. Noise can arise at various stages in the measurement process, including the sensor signal under measurement, the sensors, the analog processing system, the data acquisition stage and the digital signal processing system out of which the noise in the early measurement stages is most harmful as it propagates and can be potentially amplified through the subsequent stages in the signal pathway. Noise can also arise in the latter stages of the signal pathway, primarily during the analog-to-digital conversion, when the continuous sensor signals are converted into a discrete subset of values and stored in the computer memory. On the other hand, the inherent drift and poor repeatability of sensor responses can also sometimes be significantly larger than most of the other noise sources effectively limiting the sensitivity of electronic nose systems.

## **2.1 Temperature Modulation:**

The selectivity of MOS gas sensors is greatly influenced by the operating temperature of the device, since the reaction rates for different volatile compounds and the stability of adsorbed oxygen species are a function of surface temperature. The performance of the MOS gas sensors can be enhanced by improving the temperature-selectivity dependence. The temperature of the sensor may be cycled during the exposure to an odorous compound to obtain multivariate dynamic responses. Several approaches have been explored for deriving higher numbers of features by applying modulated temperature to the sensor instead of applying a fixed temperature<sup>114-117</sup>. Application of periodic heating voltage to MOS gas sensors has several advantages:

- i) Because of different rates of reaction of various gases at different temperatures, a cyclic variation of temperature gives a unique signature for each gas.
- ii) Sensitivity and selectivity may be enhanced.

Usually it is seen that applications such as pattern recognition and multi-component analysis are done with fixed temperature of the sensor heater, which leads to lack of selectivity and discrimination capability of the sensor. Many authors have indicated that modulation of the sensor temperature<sup>114-116</sup> provides more information from a single sensor than in isothermal operation, allowing improved research works in gas detection. Authors have reported on the advantage of temperature modulation of MOS gas sensor at two different temperatures to detect the presence of carbon mono-oxide<sup>19, 118, 119</sup>. Work has been carried on the temperature modulation using square wave to quantify hydrogen sulphide by many researchers<sup>21, 22</sup>. To discriminate between different gases, modulating waveforms such as sawtooth, triangular and square were also applied to the sensors<sup>23</sup>. The sinusoidal variation in the temperature also enhanced the identification of different gases. A number of works on the cyclic variations of the sensor heater have been reported by many authors<sup>120, 121</sup>. In the temperature cycling technique, the heating element of the gas sensor is connected to a waveform generator that periodically changes the working temperature of the device. The development of micromachined substrates for MOS gas sensors ensured operating temperature modulated in a more efficient way. Cavicchi *et al* introduced the use of micromachined tin oxide gas sensors in temperature modulation applications<sup>26-28</sup>. The temperature profile of the sensor surface greatly influence the response behavior due to rapid thermal fluctuations in respect of its noise and stability. Researchers have tried to improve selectivity by modulating the heater voltage however analysis of noise and stability of the sensor responses under modulated heater voltage has not been explored so far. Therefore the aim of this research is to analyse the baseline noise behavior and stability of MOS gas sensors by applying pulse voltages to the heater with different frequencies and duty cycles.

### **2.1.1 Experimental set-up:**

In this research work, noise feature analysis of MOS gas sensors under pulse temperature modulation is achieved. Three MOS gas sensors, TGS-2611, TGS-822 and TGS-842 of FIGARO INC, Japan (Table 2.1) are used to carry out the experiments for noise feature analysis. Based on its sensitivity to different odours such as alcohol, volatile organic compounds (VOCs) etc the sensors are selected. The three MOS gas sensors are supplied with the gases through the teflon pipes. The different gases used in the experiment are *ethyl acetate, acetonitrile, ethanol, kerosene, petroleum ether,*

*chloroform, methanol, isopropyl alcohol, acetone and hexane.* The description of each of the gases is tabulated in Table 2.2.

**Table 2.1:** Details of the Sensors used in Experiments

Sensors Range	Manufacturer	Specific Use	Detection Range
TGS-2611	Figaro Engineering Inc.	Combustible gas detection. Sensitive to Methane, Acetonitrile, Kerosene, Petroleum ether, Chloroform, Methanol, Acetone, Hexane etc.	500 to 10,000 ppm
TGS-822	Figaro Engineering Inc.	Organic solvents such as alcohol (ethanol, isopropylalcohol, methanol etc.), toluene etc.	50 to 5,000ppm
TGS-842	Figaro Engineering Inc.	Combustible gas detection. Sensitive to acetonitrile, chloroform, methanol, acetone hexane etc.	500ppm to 10,000ppm

**Table 2.2:** Composition of the ten sample gases:

Sl. No.	Gases Used	Description
1.	Ethyl-acetate (CH <sub>3</sub> COOCH <sub>2</sub> CH <sub>3</sub> )	It is an organic compound and is the ester of ethanol and acetic acid.
2.	Acetonitrile (CH <sub>3</sub> CN)	It is the simplest organic nitrile and also termed as methyl cyanide.
3.	Ethanol (CH <sub>3</sub> CH <sub>2</sub> OH)	It is a 2-carbon alcohol and also termed as ethyl-alcohol.
4.	Kerosene	It is a combustible hydrocarbon liquid constituting of n-dodecane, alkyl benzenes, and naphthalene and its derivatives.
5.	Petroleumether	It is a light hydrocarbon comprising of a mixture of alkanes, e.g., pentane, hexane, and heptanes.
6.	Chloroform (CHCl <sub>3</sub> )	It is an organic compound produced by heating a mixture of chlorine and either chloromethane or methane.
7.	Methanol (CH <sub>3</sub> OH)	It is the simplest alcohol and also termed as methyl-alcohol.

8.	Isopropylalcohol (C <sub>3</sub> H <sub>8</sub> O)	It is the simplest example of a secondary alcohol, where the alcohol carbon is attached to two other carbons. It is a structural isomer of propanol.
9.	Acetone ((CH <sub>3</sub> ) <sub>2</sub> CO)	It is also termed as dimethyl-ketone and is produced directly or indirectly from propylene.
10.	Hexane (C <sub>6</sub> H <sub>14</sub> )	It is a hydrocarbon or an alkane with six carbon atoms.

The sensor TGS-2611 has a very high sensitivity to methane gas. The target gases for this type of sensor are methane and natural gases. So the sensor has sensitivity towards gases such as *acetonitrile*, *kerosene*, *petroleum ether*, *chloroform*, *methanol*, *acetone* and *hexane*. TGS-822 has high sensitivity to the vapors of organic solvents as well as other volatile vapors. It also has sensitivity to a variety of combustible gases. Hence the sensor has good sensitivity towards the gases such as *ethanol*, *isopropylalcohol*, and *methanol*. Similarly, TGS-842 has high sensitivity and selectivity to methane and natural gases (naturally occurring hydrocarbon gas mixture). The gases such as *acetonitrile*, *chloroform*, *methanol*, *acetone* and *hexane* therefore are sensitive to this sensor.

Diaphragm pumps are used to direct the sample gas and the clean air flow into the sensor headspace. The pumps are controlled by the PC through a driver circuit consisting of relays and transistor switches. The sequence of ‘purging’ and ‘refreshing’ with proper time duration was controlled through the DAQ card by the PC using LabVIEW programming. The sensors used are shown in Fig.2.1. The experimental set-up consists of these three sensors and a diaphragm pump system with flow control devices.



**Fig. 2.1.** Three Taguchi Gas Sensors from Figaro Inc. Japan, used in this Research Work.

The experiment is conducted on the MOS gas sensors for different pulse modulating temperature. The modulation patterns of heater voltage (frequency and duty cycle) of the sensors are controlled by a PC through a Data Acquisition (DAQ) card PCI6024E, National Instruments) and data acquisition software-LabVIEW. Analog output of the card was applied to the gate of a MOSFET which supplies the pulse modulating voltage to the heaters of the sensors. Therefore, the heater voltage ( $+V_H$ ) accordingly followed the pulse signal to excite the sensor. The sensor output was interfaced to the PC through the DAQ card. The sensors are kept inside a sensor head chamber away from interfering gas so that the baseline is established with clean air. Before each run of data acquisition, the baseline was verified and when found deviated, it was corrected by applying clean air. It was found in each run of experiment that on application of clean air the sensor baseline settles to a fixed level ensuring absence of any interfering gas. When the pulse signal generated by the PC switches on the MOSFET, the heater voltage is switched on to +5 V with the same frequency as that of the pulse applied. As a result the sensor temperature becomes pulsating with different frequencies. Fig 2.2 shows few typical signals used for modulating the heater temperature; however the pulse (b) signal was used for the experiment.

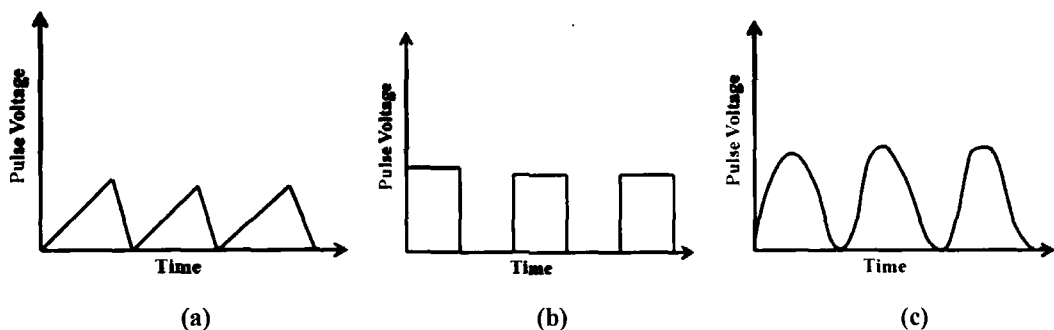


**Fig. 2.2** Typical signals (a) ramp, (b) pulse and (c) sinusoidal used for modulating the heater temperature .

Ideally, the reference and sample vessels are placed in controlled room environment at about 25°C temperature and 65% humidity with deviation less than  $\pm 2\%$ . The switching circuits are developed using 12 V relay (**Series 511, SPDT**) for alternately switching between reference vessel and sample vessel. The sequence of 'purging' and 'refreshing' with proper time duration was controlled through the DAQ card by the PC using LabVIEW programming. The two transistors used for switching are **BD139**. Two diaphragm pumps (**SB-548A**) are used for constant supply of sample vapour and room

air as desired by the programmed options. Data acquisition of the sensor signals is performed by High Performance data Acquisition Card (PCI-6024E, National Instruments). The card has also been used to condition the data in required format and convert into digital form to make it compatible with computer processing. The photograph of the sensor set-up is shown in Fig.2.3.

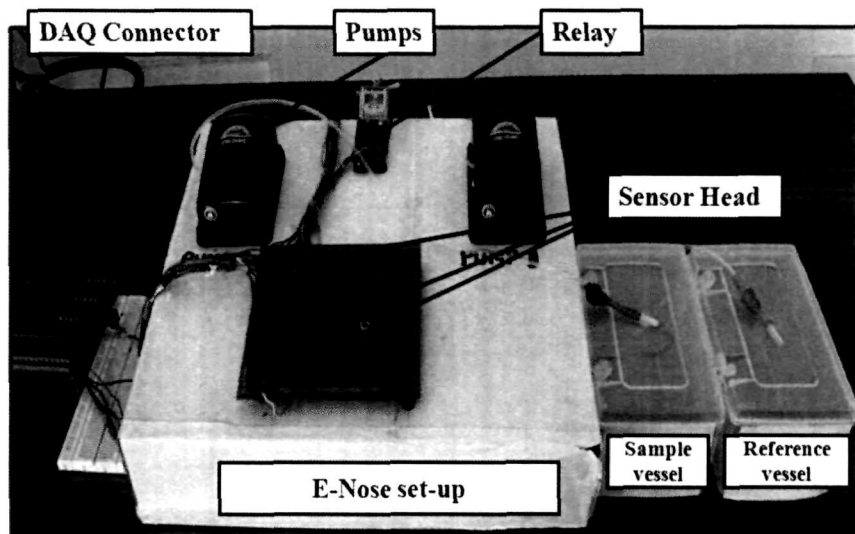


**Fig. 2.3:** MOS Gas sensor Experimental set-up, Department of Electronics & Comm.Engg., Tezpur University, India.

## 2.2 Noise parameters analysis:

Research has been carried out on the noise in sensors<sup>122, 123</sup> and different techniques have been developed for selectivity detection of gases<sup>124</sup>. Determination of noise features such as Probability Distribution Function (PDF) and power density spectrum estimation has been performed for several typical gas sensors<sup>125</sup>. The noise feature analysis for typical gas sensors have been performed by many researchers during the past years. Fengchun Tian et al<sup>126</sup> determined the noise features of gas sensors due to fixed sensor temperature; however noise analysis under modulated temperature has not yet been performed. The reason for analyzing the sensor noise behavior at different frequencies and duty cycles is that we need to know a suitable pulse frequency and duty cycle at which the sensor can be used with the best signal to noise ratio (SNR). This is important in circumstances where a sensor has to discriminate or classify odours in a noisy environment. In this work, pulse modulated heater voltage with different frequencies and

duty cycles were applied to the heater of the MOS gas sensor heater to achieve the modulation in the sensor temperature for studying the type of noise. The frequency spectrum of noise was determined by FFT analysis and noise dependency was verified by PDF, histogram and SNR under different frequencies and duty cycles of pulse heater voltage. Fig.2.4 shows the pulse modulating and DAQ system.

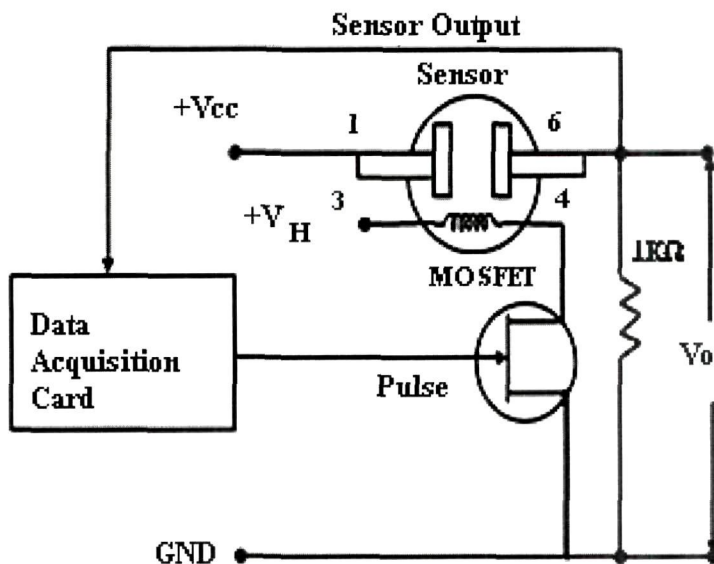


**Fig. 2.4.** Pulse modulating and DAQ system.

### 2.2.1 Data Acquisition:

In this research, we have conducted sensor noise analysis by two different experiments-

- a) In the first part of the experiment, the data acquisition and storage was done without the application of any input odour to the MOS gas sensor.
- b) Based on the experiment (a), the best selected frequency and duty cycles are used to show the classification efficiency. The analysis is conducted on the acquired signals by applying ten different gases- acetone, acetonitrile, chloroform, ethanol, ethyl acetate, isopropylalcohol, kerosene, methanol, n-hexane and petroleumether.

The flow rates are kept constant for both of the two experiments. The schematic diagram for the flow control and alternate switching for sample and reference gases is shown in Fig.2.5. The gases were selected based on the fact that the MOS gas sensors used (TGS-

2611, TGS-822 and TGS-842) have good sensitivities to the families of the gases as described in *Section 2.1.1*.

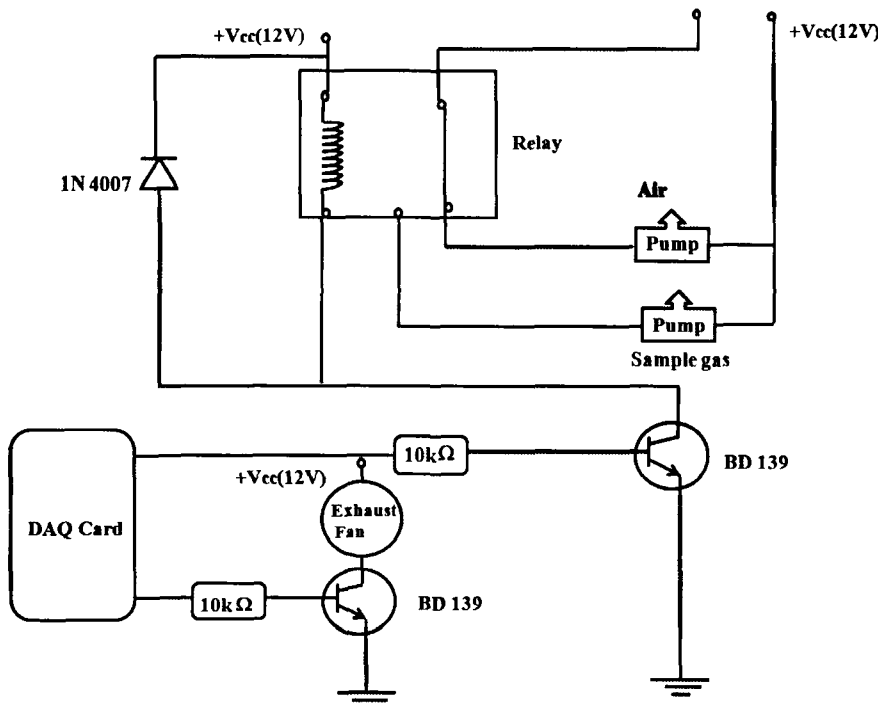


**Fig. 2.5.** Pump control driver circuit for switching between sample and reference vessels.

### 2.2.1.1 LabVIEW Environment

LabVIEW features interactive graphics, a state-of-the-art user interface, and a powerful graphical programming language. In the LabVIEW DAQ VI Library, a series of virtual instruments for using LabVIEW with National Instruments DAQ hardware, is included. The devices have three different input modes—non referenced single-ended (NRSE), referenced single-ended (RSE), and differential (DIFF) input. The single-ended input configurations provide up to 16 channels while the DIFF input configuration provides up to eight channels. Input modes are programmed on a per channel basis for multimode scanning. Connection of these analog input signals to the device depends on the type of input signal source and the configuration of the analog input channels used. When configuring the input channels and making signal connections, we determine whether

the signal sources are floating or ground-referenced. A ground-referenced signal source is connected to the building system ground and is, therefore, already connected to a common ground point with respect to the device, assuming that the computer is plugged into the same power system. In our case we configure the input channel in the RSE mode. The devices have a bipolar input range that changes with the programmed gain. The devices can scan multiple channels at the same maximum rate as their single-channel rate. They supply two channels of analog output voltage at the I/O connector. The bipolar range is fixed at  $\pm 10$  V. Data written to the digital-to-analog converter (DAC) is interpreted in two's complement format. The block diagram configured in LabVIEW is shown in Fig 2.6. For measurement task, the simulated signal was configured as 'Output to DAQ assistant2'. The 'Write to Measurement file' was configured for storing the data which was saved as LVM files. The sensor responses were observed in the front panel.

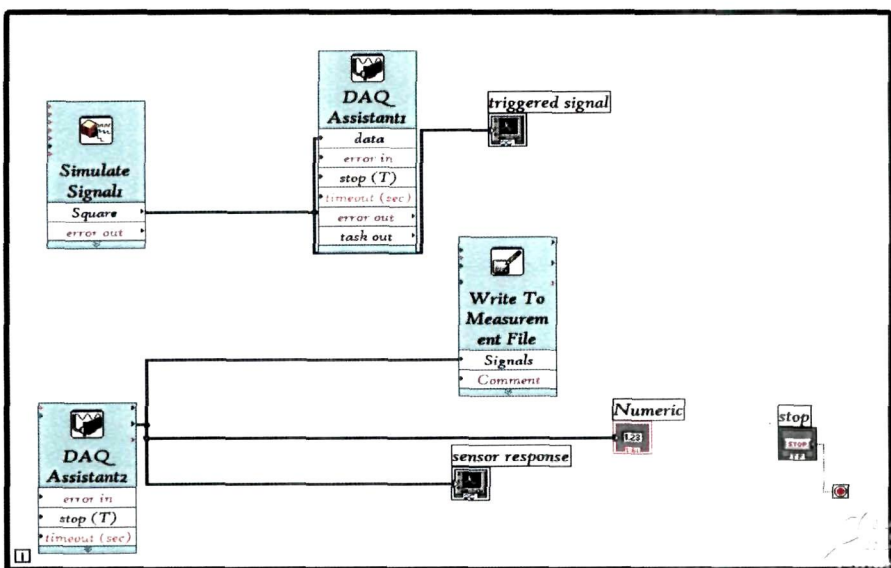


Fig. 2.6 Block diagram configured in LabVIEW.

### 2.2.1.2 Heater Voltage Modulation

A pulse signal whose duty cycle and frequency can be controlled was generated in the LabVIEW environment and applied to the sensor heater through a MOSFET. As a result the sensor temperature becomes pulsating with different 'on' and 'off' durations. The sensor output signal captures noise developed inside the sensor which is mostly thermal

noise. The sensor response was analyzed without applying any gas for noise with the pulsed heater voltage applied. The frequency and the duty cycle of the heater ‘on’/ ‘off’ sequence was varied to analyze the noise behavior.

The sensor temperature was pulsed at four selected frequencies of 10 mHz, 40 mHz, 80 mHz and 120 mHz to generate noise. Further the noise behavior was analyzed with two different ‘on’ and ‘off’ time durations i.e. duty cycle of the pulse signal- 50 % and 75 % duty cycles without the application of any gas. The MOS gas sensor noise analysis under signal inactive period i.e. without application of gas is important to determine suitable time duration of the pulsed heater voltage at four different heater pulse frequencies. Therefore the frequency and duty cycle of the heater pulse voltage is required to be correlated to severity of noise. The sensor responses were acquired at a sampling frequency of 1 kHz over duration of about 15 min, so that sufficient data is available for analysis. The pulse frequency and duty cycle were varied for each experiment after correcting the baseline. In order to avoid non-uniformity, data for a single pulse cycle was extracted and analyzed in MATLAB.

Normalization of data was performed to highlight the noise spectrum over a positive scale. FFT, PDF, histogram, other statistical parameters (mean, standard deviation and variance) and SNR were calculated. The total data points for the signals with frequencies of 10 mHz, 40 mHz, 80 mHz and 120 mHz were  $100 \times 10^3$ ,  $25 \times 10^3$ ,  $12.5 \times 10^3$ ,  $8 \times 10^3$  respectively at the sampling frequency used in the experiments.

### 2.2.1.3 Measuring Circuit

The application circuit diagram for measuring the MOS gas sensors response is shown in Fig.2.7. The resistances and power supplies indicated in Fig.2.7 are as follows:

#### i) Sensor Resistance ( $R$ )

This is the characteristic resistance of the sensor surface normally defined by the manufacturer in a range under standard ppm of certain sample and other circuit conditions of load resistance and power supply ( $V_c$ ). The value  $R$  changes on exposure to different sample vapors. The typical values are  $(1-5)k\Omega$  for TGS-2611,  $(1-10)k\Omega$  for

TGS-822 and (3-15)k $\Omega$  for TGS-842. The output response is generated by the change in the resistance of the sensor surface on application of a gas.

### **ii) Load Resistance ( $R_L$ )**

The load resistance is selected based on the condition that the power dissipation does not exceed the limit specified by the manufacturer for the sensors. The resistance values are calculated for the three sensors based on the maximum current under minimum sensor resistance ( $R$ ). The values are indicated in the circuit diagram of Fig.2.7 and listed in Table 2.3.

### **iii) Circuit Power Supply ( $V_c$ )**

The maximum circuit power supply specified by manufacturer for the three sensors is 24V. In this circuit, the used value of  $V_c$  is 12V.

### **iv) Heater Voltage ( $V_H$ )**

The heater voltage is a uniform value of 5V for all the three sensors which keeps the sensors at elevated temperature of 200 to 400°C (approx.) to have better response.

### **v) Output Voltage ( $V_o$ )**

The output voltage is measured as the sensor response across the load resistance  $R_L$  which varies from a fraction of a volt to few volts.

### **vi) Power Dissipation ( $P_s$ )**

The maximum power dissipation takes place when the sensor resistance ( $R$ ) is minimum for chosen load resistance and power supply. The power dissipation is given by -

$$P_s = (V_c^2 \times R_s) / (R_s + R_L)^2$$

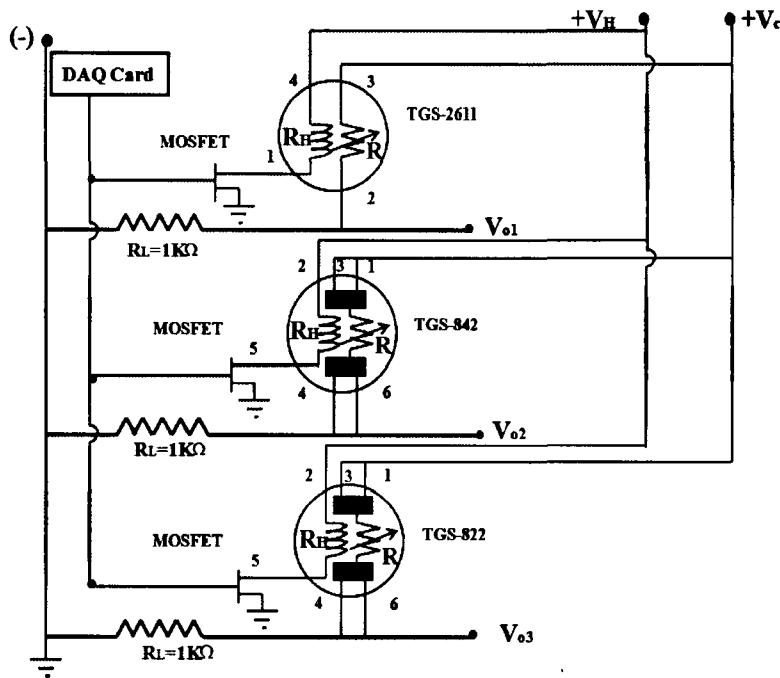


**Fig. 2.7 Measurement Circuit for MOS gas sensor responses.**

#### 2.2.1.4 E-Nose set-up

The E-Nose system of this work comprises of three MOS gas sensors namely TGS-2611, TGS-822 and TGS-842. The interfacing with the PC is done in order to achieve the online acquisition of E-Nose sensor responses in real time and providing control signals to the E-Nose electronic circuits for various operations such as switching and time setting. The E-Nose set up interfacing with PC is shown in Fig.2.8.

#### 2.2.2 Data Pre-processing:

The pre-processing of the data is done for the following reasons-

- i) to reduce the amount of data which are irrelevant to the study;
- ii) to enhance sufficient information within the data to achieve the desired goal;
- iii) to transform the data to a form suitable for further analysis.

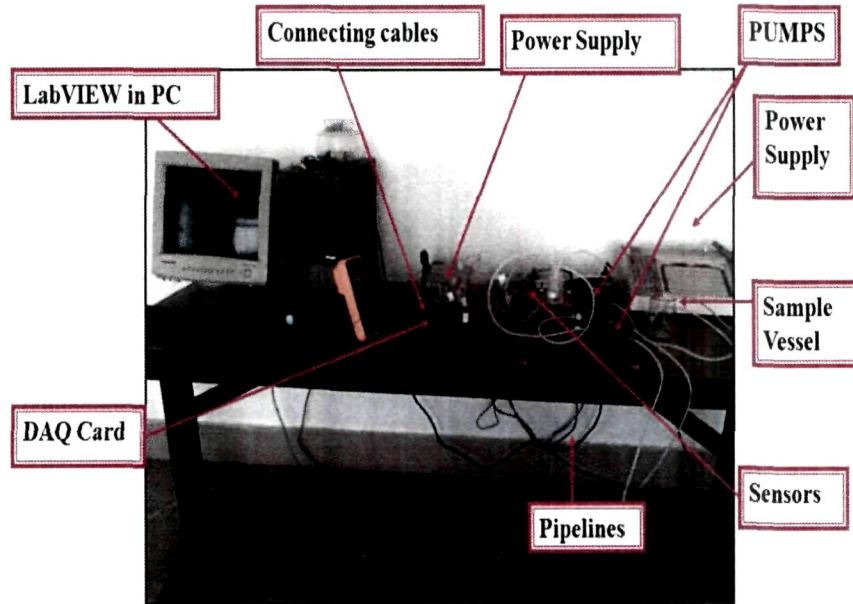


**Fig. 2.8** E-Nose set up interfacing with PC.

Various analytical methods are used for the pre-processing of data out of which the common one is the vector normalization method. Since the sensors in the E-Nose array have different sensitivities, the voltage levels of the output signals from the sensors will be different. Hence the signal levels need a standardization or normalization. Normalization removes sample-to-sample absolute variability and transforms vector length to be one. It assumes that the extracted features linearly correlate with signal intensity. Various methods of normalizations are available such as-

**a) Liberalization:**

$$X_{ij} = \log |(Y_{ij}^{\max} - Y_{ij}^{\min})| \quad (2.1)$$

$$X_{ij} = \sqrt{|(Y_{ij}^{\max} - Y_{ij}^{\min})|} \quad (2.2)$$

**b) Vector Normalization:**

$$R_{ij} = X_{ij} / \sum (X_{ij})^2 \quad (2.3)$$

**c) Sensor Normalization:**

$$R_{ij} = X_i / \max(X) \quad (2.4)$$

**d) Sensor Auto Scaling:**

$$R_y = \left| (X_y - X_y^{mean}) \right| \sigma_i \quad (2.5)$$

where  $\sigma$  is the standard deviation.  $X$ 's are the calculated or preprocessed values and  $Y$ 's are the observed or measured values for sample odour and  $Y_y^{\max}$  and  $Y_y^{\min}$  are its maximum and minimum values.

**Table 2.3:** MOS gas sensor parameters.

Sensor	$V_H$ (V)	$V_c$ (V)	Sensor Resistance $R(k\Omega)$	Heater Resistance $R_H(\Omega)$	Heater Current $I_H(mA)$	$R_L$ ( $k\Omega$ )	Max.Power Dissipation ( $P_s$ ), for $R$ (min) (Worst condition)	Target Gases
TGS- 2611	5	5	0.68 to 6.8 in 5000 ppm	59	$56 \pm 5$	1	12.5mW	Methane, Natural Gas
TGS- 822	5	5 or 10	1 to 10 in 300ppm	38	132	1	12.5mW	Alcohol Organic solvents
TGS- 842	5	5 or 10	5 to 20 in 1,000ppm	30	167	1	4.68mW	Methane Natural gas

The normalised data are stored in the memory for pattern recognition. Most widely used normalization technique is the vector normalization where each feature vector is divided by its mean so that it is transformed to lie on a hyper-sphere of unit value. We have used sensor normalization technique (eqn.2.4) to normalize the sensor data for noise feature analysis.

### 2.3 Statistical analysis:

The MOS gas sensor noise analysis under signal inactive period i.e. without application of gas is important to determine a suitable time duration of the pulsed heater voltage at four different heater pulse frequencies. Therefore the frequency and duty cycle of the heater pulse voltage is required to be correlated to severity of noise. Here we have tried to observe and analyse the noise in the MOS gas sensors with the sensor excited by its power supply ( $V_c$ ) and pulse modulated heater voltage ( $V_H$ ) without applying any gas.

From the sensor data response, a single data set  $X$  is constructed for all the four different frequencies i.e. 10mHz, 40mHz, 80mHz and 120mHz and two duty cycles of 50% and 75%. The LabVIEW display of sensor TGS-822 for 10mHz and 50% duty cycle is shown in Fig. 2.9. The noisy responses of the gas sensors TGS-822, TGS-842 and TGS-2611 for all the four frequencies and two duty cycles, in MATLAB are shown in Fig.2.10.

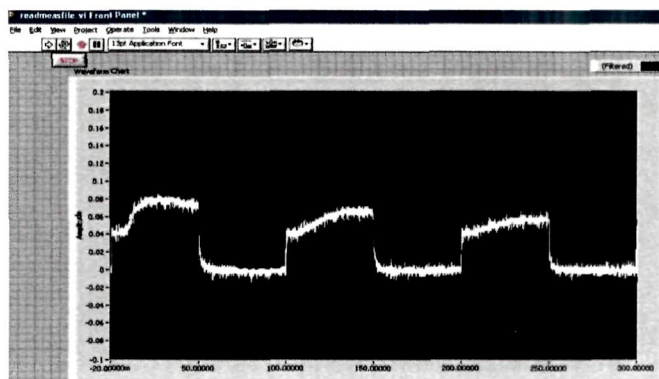
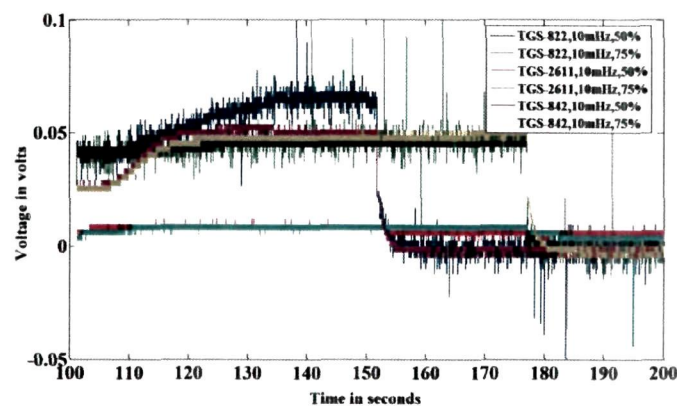


**Fig. 2.9.** Noisy response shown by sensor TGS-822 in LabVIEW at 10mHz and 50% duty cycle.



(a)

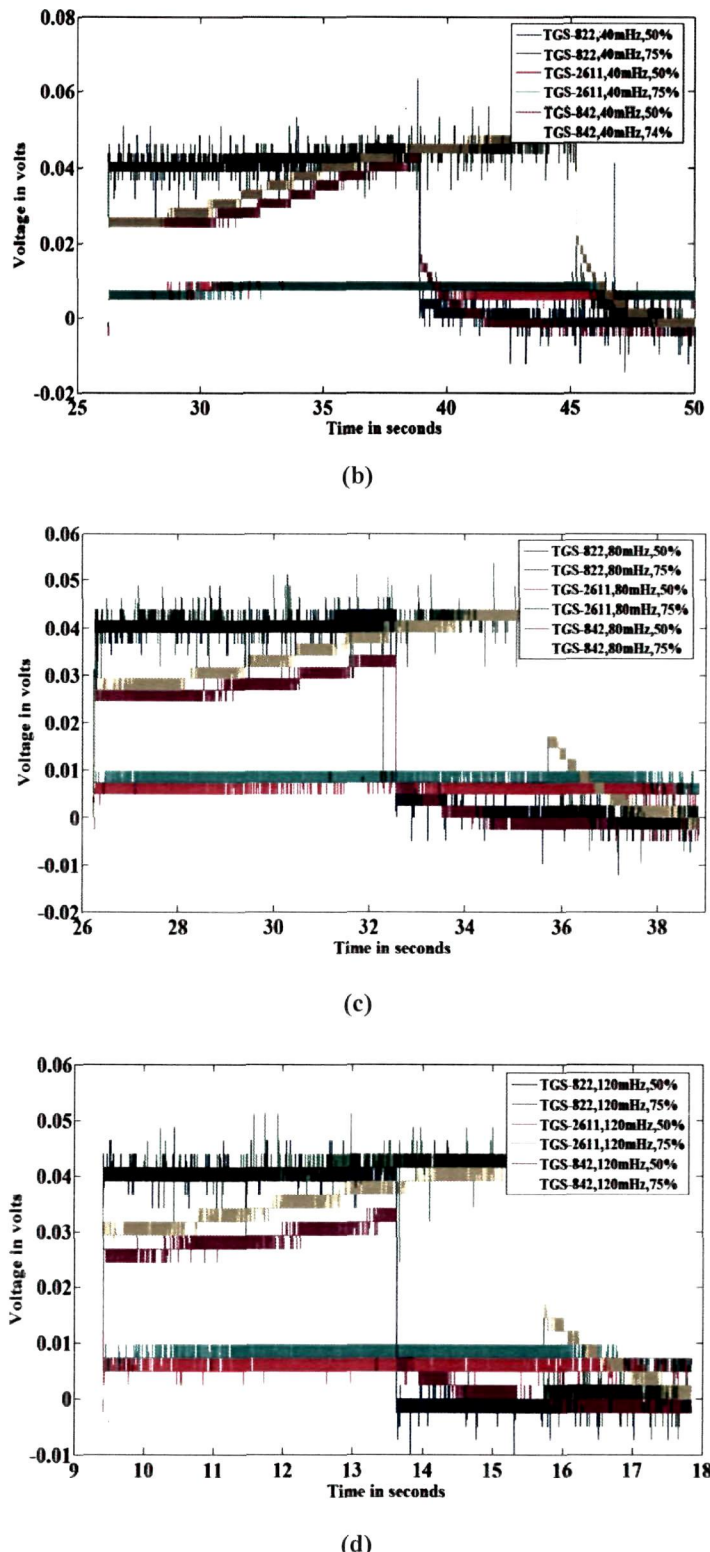


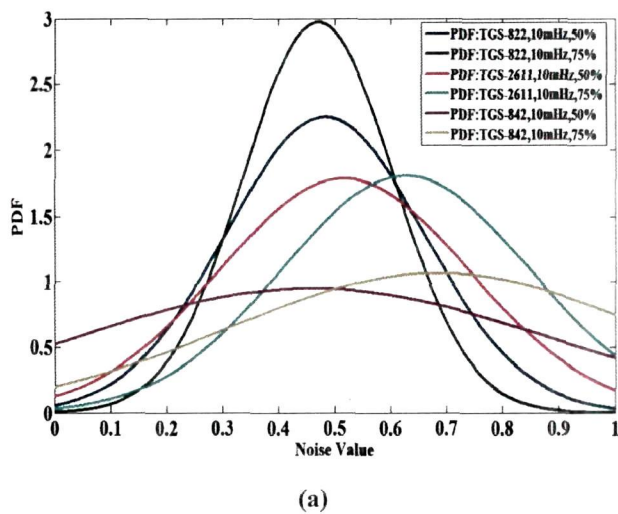
**Fig. 2.10.** Noisy responses of TGS-822, TGS-2611 and TGS-842 at 50% and 75% duty cycles for (a) 10mHz, (b) 40mHz, (c) 80mHz and (d) 120mHz.

The data vector has been constructed for each sensor comprising of two columns- the time-column (x-axis) and the sensor voltage (y-axis). The y-column vector was used to compute the FFT of the sensor data in MATLAB.

### 2.3.1 Probability distribution function (PDF):

PDF is an important statistical tool to analyze the noise characteristics of a sensor signal. The theory of probability gives us the basic tools for constructing and analyzing mathematical models for random phenomena such as noise.

In this chapter, noise analysis under modulated temperature is performed. Pulse modulated heater voltage with different frequencies and duty cycles are applied to the MOS gas sensor heater to achieve the modulation in the sensor temperature for studying the type of noise. The frequency spectrum of noise is determined by FFT analysis and noise dependency is verified by PDF, histogram and Signal-to-Noise Ratio (SNR) under different frequencies and duty cycles of pulse heater voltage. The normalized data from the sensors is used to compute the PDF estimation and histogram. The noise PDF shows that for all cases of pulses, the distribution is Gaussian however with different mean, variance and standard deviation. The PDF for the sensor noise signals satisfies the requirement for the noise to be coloured i.e. with non-zero mean. Fig. 2.11 shows the PDF of TGS-822, TGS-842 and TGS-2611 at 10mHz, 40mHz, 80mHz and 120mHz each at 50% and 75% duty cycles respectively.



(a)

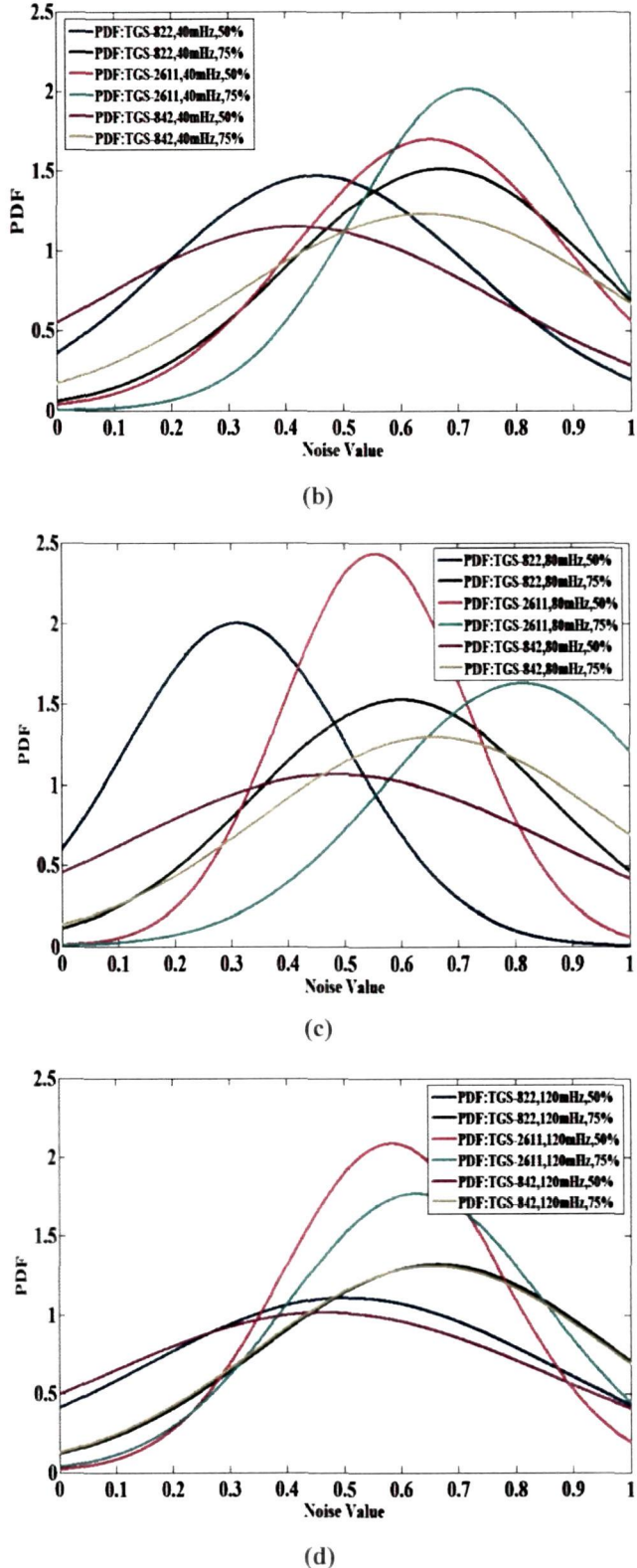


**Fig. 2.11.** The PDF of TGS-822, TGS-2611 and TGS-842 sensor noise signals at 50% and 75% duty cycles for (a) 10 mHz , (b) 40 mHz, (c) 80mHz and 50% duty cycle, and (d) 120mHz.

### 2.3.2 Histogram:

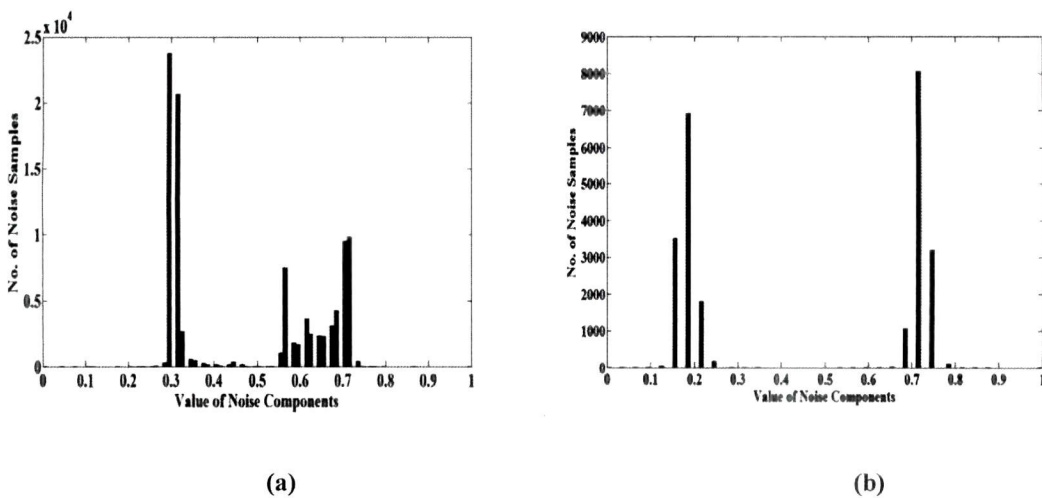
Histogram is a graphical representation showing a visual interpretation of the distribution of data. The histogram is used to group sensor response voltages together that have the same value. The histogram method, which has been proved to be an unbiased estimation for a random variable, is used to estimate the PDF of noise<sup>127</sup>. Typically, the histogram results a Gaussian distribution when the number of samples is large. Hence from definition of histogram, the sum of all the values in the histogram must be equal to the number of points  $N$ , in the signal given by eqn.1.7.

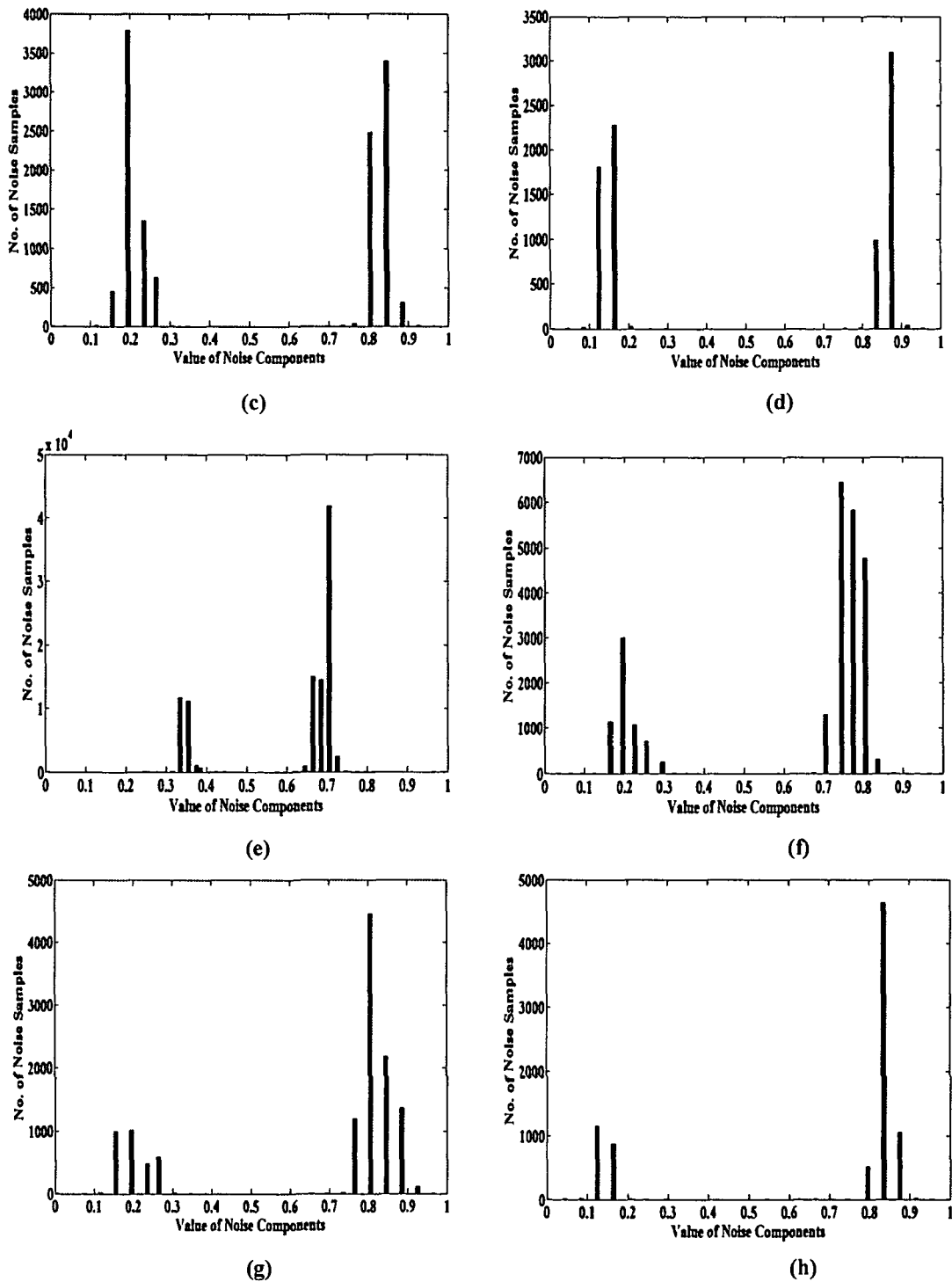
The histogram is used to calculate the mean and standard deviation of very large data sets. The mean ( $\mu$ ) and standard deviation ( $\sigma$ ) are calculated from the histogram by the equations (1.8) and (1.9).

Mathematically, a histogram is a mapping  $m_i$  that counts the number of observations that fall into various disjoint categories (known as bins), whereas the graph of a histogram is merely one way to represent a histogram. Thus, if  $n$  is the total number of observations and  $k$  be the total number of bins, the histogram  $m_i$  meets the following conditions:

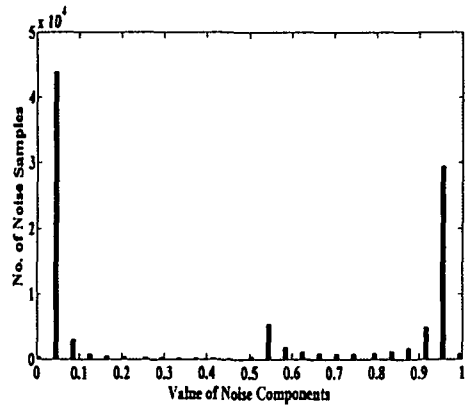
$$n = \sum_{i=1}^k m_i \quad (2.6)$$

Fig. 2.12, Fig. 2.13 and Fig. 2.14 shows the histograms of the sensor TGS-822, TGS-842 and TGS-2611 for the same respective frequencies and duty cycles.

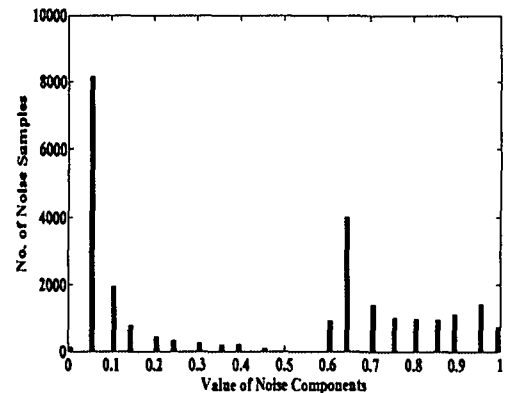




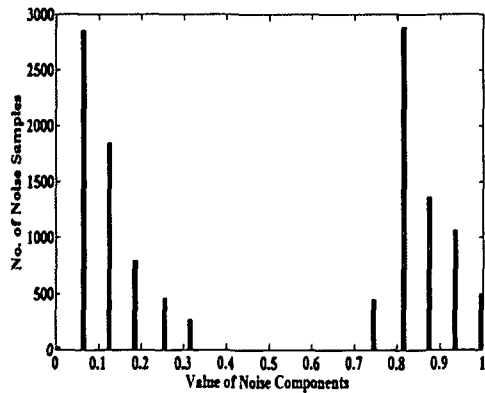
**Fig. 2.12.** The histogram of TGS-822 sensor noise signals at (a) 10 mHz and 50% duty cycle, (b) 40 mHz and 50% duty cycle, (c) 80mHz and 50% duty cycle, (d) 120 mHz and 50% duty cycle, (e) 10 mHz and 75% duty cycle, (f) 40 mHz and 75% duty cycle, (g) 80mHz and 75% duty cycle, (h) 120 mHz and 75% duty cycle



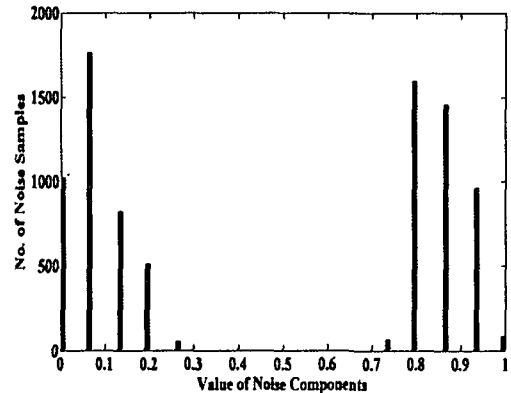
(a)



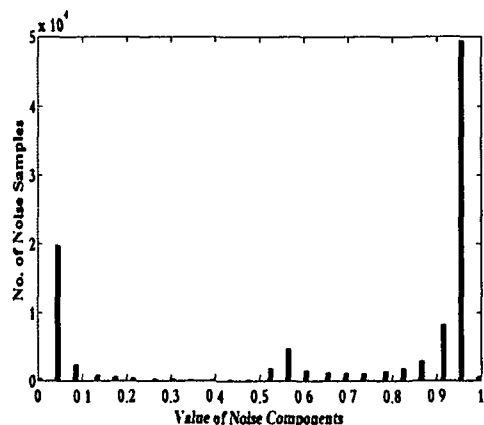
(b)



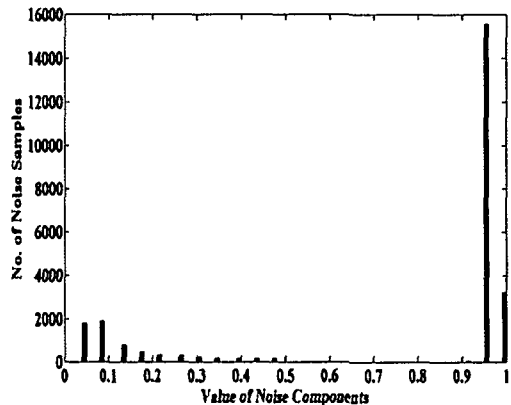
(c)



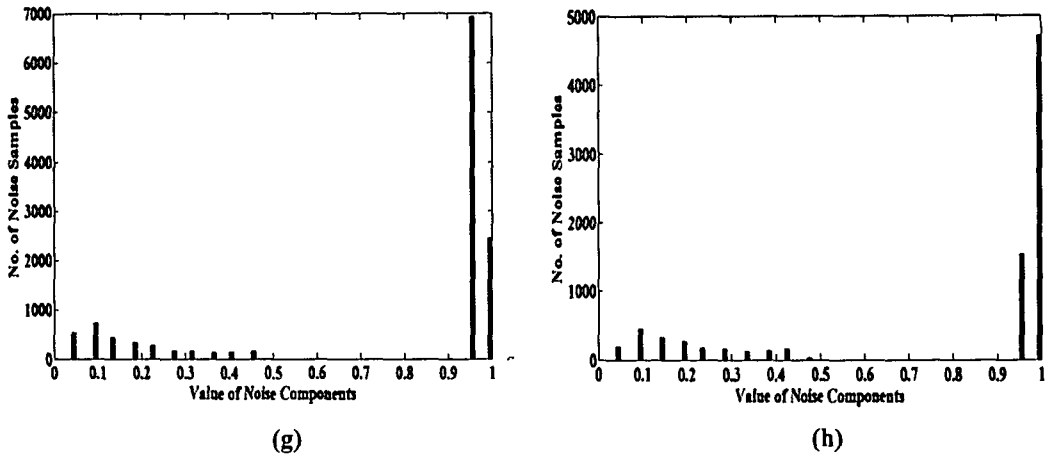
(d)



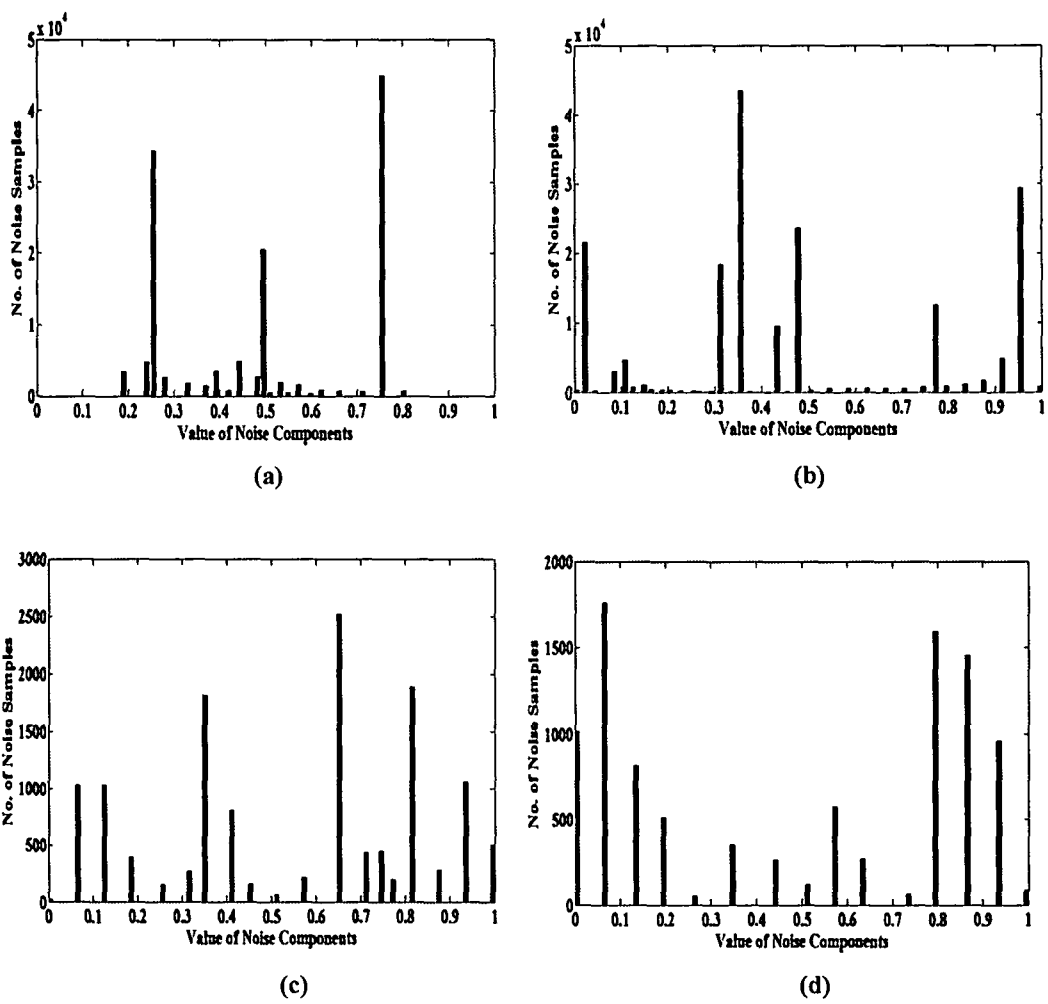
(e)



(f)



**Fig. 2.13.** The histogram of TGS-842 sensor noise signals at (a) 10 mHz and 50% duty cycle, (a) 40 mHz and 50% duty cycle, (c) 80mHz and 50% duty cycle, (d) 120 mHz and 50% duty cycle, (e) 10 mHz and 75% duty cycle, (f) 40 mHz and 75% duty cycle, (g) 80mHz and 75% duty cycle, (h) 120 mHz and 75% duty cycle.



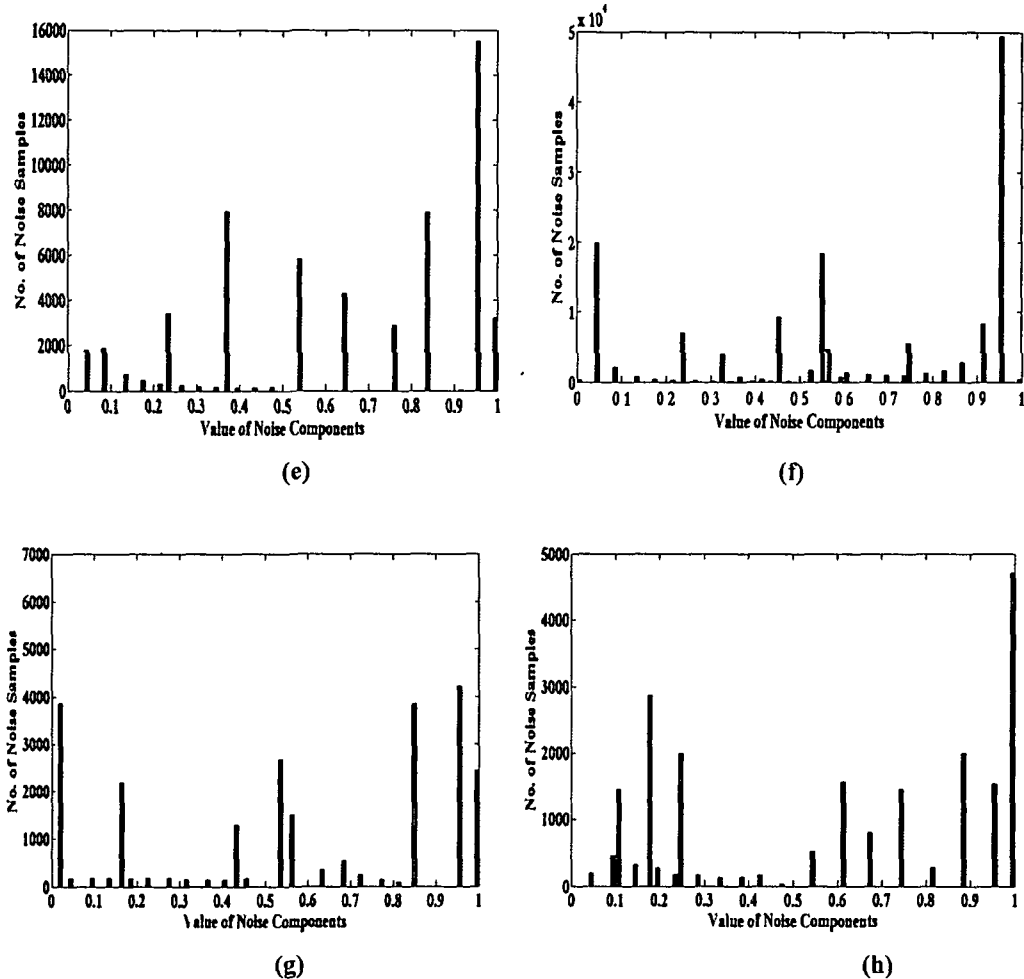


**Fig. 2.14.** The histogram of TGS-2611 sensor noise signals at (a) 10 mHz and 50% duty cycle, (a) 40 mHz and 50% duty cycle, (c) 80mHz and 50% duty cycle, (d) 120 mHz and 50% duty cycle, (e) 10 mHz and 75% duty cycle, (f) 40 mHz and 75% duty cycle, (g) 80mHz and 75% duty cycle, (h) 120 mHz and 75% duty cycle.

The mean value of the noise data showed that it is non-zero, depicting that the noise is colored and  $1/f$  type. Higher standard deviation and variance was observed when the pulse frequency was increased which showed that the signal becomes noisier for the three sensors when pulsed heater voltage frequency is increased. The duty cycle of the pulse also changes the noise level with reverse dependency i.e. noise level increases when duty cycle is reduced. Table.2.3 shows the mean, variance and standard deviation calculated for various frequencies and duty cycles for all the three sensors. From Table 2.3 it is observed that for all the three sensors, the most convenient results i.e. lowest noise is obtained at 10mHz frequency and 75% duty cycle.

### 2.3.3 Signal-to-Noise Ratio (SNR):

The *signal-to-noise ratio* (SNR) is the ratio of the signal amplitude to the noise signal amplitude at a given point in time. SNR is usually expressed in dB and in terms of peak values for impulse noise and root-mean-square values for random noise. When a signal is constant or periodic and the noise is random, it is possible to enhance the SNR by averaging the measurement. In this research, the ratio of the sensor response signal for pulsed heater voltage to the noise in the average power level is termed as the Signal-to-Noise ratio (SNR) of the sensor given by-

$$SNR = \frac{P_S}{P_N} \quad (2.7)$$

where  $P_S$  is the power of the sensor response signal and  $P_N$  is that of the noise present in the signal. Measuring the SNR usually requires that the noise be measured separately, in the absence of signal. Depending on the type of experiment, it may be possible to acquire readings of the noise alone, for example on a segment of the baseline before or after the occurrence of the signal. However, if the magnitude of the noise depends on the level of the signal, then the experimenter must try to produce a constant signal level so as to measure the noise on the signal. In a few cases, where it is possible to model the shape of the signal exactly by means of a mathematical function, the noise may be estimated by subtracting the model signal from the experimental signal.

In this work, the SNR is calculated for all the three sensors during signal inactive period i.e. without application of gas and is tabulated in Table 2.3. It can be seen, that at a particular frequency of 10mHz and 50% duty cycle, the SNR of sensor TGS-822 and TGS-842 ranges from about 45.63dB to 56.88dB. Within this particular range for the said frequency and duty cycle, the two sensors produces noise differently which is same as in the case for a different set of frequencies and duty cycle. Therefore, this analysis can be used for comparing the noise immunity of the two sensors. Similar is the case when we compare all the three sensors. From Table 2.4 it can be seen that at a frequency of 10mHz and 75% duty cycle, TGS-2611 shows the highest SNR with a value of 59.22dB as compared to TGS-822 and TGS-842.

### 2.3.4 Noise spread and population behavior:

In this study, two newly introduced noise characteristics are analyzed with the help of the histogram components of the signal and the corresponding histogram ratios. This study is found to be an additional statistical noise feature to confirm the noise dependency on the frequency and the duty cycle of the pulse modulated heater voltage.

#### 2.3.4.1 Signal spread and population behavior of MOS gas sensor

A histogram is a mathematical tool that gives only the number of samples for different signal levels. However, it is not possible to compare two histograms in terms of spread and population of the samples. In this study a new characteristic has been defined which determines the noise behavior of the three sensors at different sensor signal levels. We have introduced two terms namely Noise Spread Figure (NSF) and Noise Population Figure (NPF) with the help of various histogram components. The noise characteristics of the sensors are therefore studied with the help of the following histogram components of the signal and their ratios as depicted in Fig.2.15.

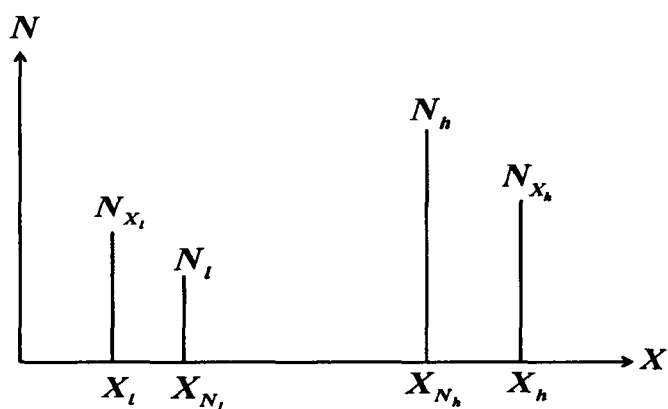


**Fig. 2.15.** Histogram showing signal spread and population.

The following histogram components can be defined as –

$X_h$  = Highest value of signal component.

$X_l$  = Lowest value of signal component.

**Table 2.4.** Bandwidth, mean, variance , standard deviation and SNR of sensor data for different frequencies and duty cycles (best suitable values are shown in bold).

Sensor	Duty cycle	Pulse Frequency (mHz)	Mean	Variance	Standard deviation	Signal-to-Noise Ratio(dB)	Noise Bandwidth (mHz)
TGS-822	50%	10	0 4830	0 0316	0 1777	45 63	7
		40	0 4542	0 0735	0 2711	41 90	19
		80	0 5189	0 0989	0 3145	34 29	38 3
		120	0 5067	0 1290	0 3592	27 32	70
	75%	10	<b>0.6057</b>	<b>0.0230</b>	<b>0.1515</b>	<b>52.04</b>	<b>3.63</b>
		40	0 6270	0 0606	0 2461	45 84	16 3
		80	0 6683	0 0743	0 2726	44 88	32 7
		120	0 6632	0 0911	0 3018	29 18	64
TGS-842	50%	10	0 4603	0 0776	0 3214	56 88	dc
		40	0 4275	0 1241	0 3523	48 05	
		80	0 4893	0 1403	0 3746	44 03	
		120	0 4700	0 1540	0 3924	27 82	
	75%	10	<b>0.6846</b>	<b>0.0605</b>	<b>0.3149</b>	<b>57.50</b>	dc
		40	0 6454	0 1058	0 3252	55 49	
		80	0 6699	0 1201	0 3465	49 76	
		120	0 7028	0 1287	0 3545	46 61	
TGS-2611	50%	10	0 5267	0 0492	0 2218	48 30	dc
		40	0 5398	0 0543	0 2330	41 03	
		80	0 5221	0 0582	0 2374	33 52	
		120	0 5188	0 0605	0 2413	30 79	
	75%	10	<b>0.8270</b>	<b>0.0458</b>	<b>0.2110</b>	<b>59.22</b>	dc
		40	0 8239	0 0489	0 2139	49 53	
		80	0 8312	0 0566	0 2279	39 99	
		120	0 8463	0 0576	0 2336	33 75	

$X_{N_h}$  = Signal value corresponding to the highest number.

$X_{N_l}$  = Signal value corresponding to the lowest number.

$N_h$  = Signal population for highest signal spread.

$N_l$  = Signal population for lowest signal spread.

$N_{X_h}$  = Samples corresponding to highest signal value.

$N_{X_l}$  = Samples corresponding to lowest signal value.

The following ratios are also defined as follows-

$$\frac{X_h}{X_l} = \text{Spread ratio of the highest to lowest components of signal value level in the histogram.} \quad (2.8)$$

$$\frac{X_{N_h}}{X_{N_l}} = \text{Spread ratio of the signal values corresponding to the highest to lowest numbers.} \quad (2.9)$$

$$\frac{N_h}{N_l} = \text{Ratio of the highest to lowest signal population.} \quad (2.10)$$

$$\frac{N_{X_h}}{N_{X_l}} = \text{Ratio of signal population for highest to lowest signal spread} \quad (2.11)$$

To analyze the signal spread and population behaviour, the following two terms are defined as:

$$\text{Noise Spread Figure (NSF)} = \frac{X_h/X_l}{X_{N_h}/X_{N_l}} \quad (2.12)$$

$$\text{Noise Population Figure (NPF)} = \frac{N_{X_h}/N_{X_l}}{N_h/N_l} \quad (2.13)$$

To explain the two figures introduced in eqn. (2.12) and (2.13), we consider a pure and a noisy signal as shown in Fig. 2.16 (a) and (b) and the components of the pure and noisy signal in 2.16 (c) and (d) respectively.

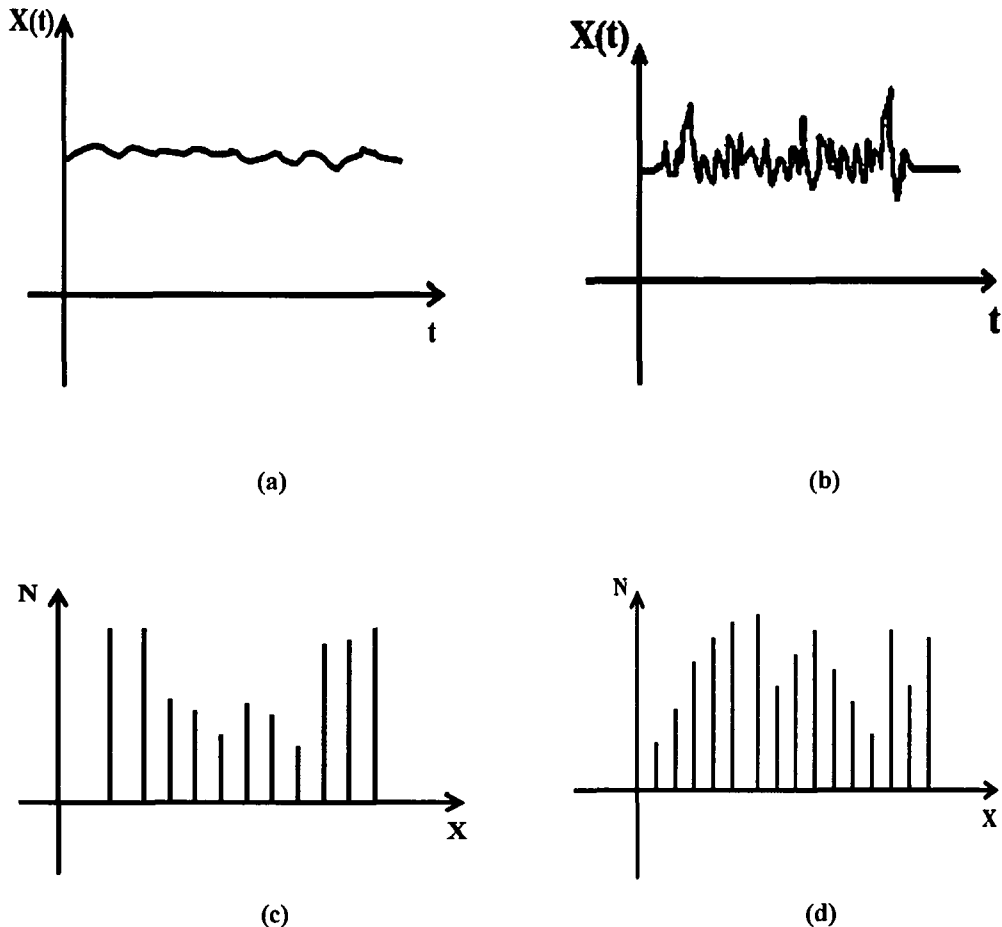


**Fig. 2.16. (a) Pure Signal, (b) Noisy Signal, (c) Histogram components of a pure signal and (d) Histogram components of a noisy signal.**

Four cases can be considered for the two cases of signals shown above:

- Case I: For a pure signal,  $X_{Nh} \gg X_{Nl}$ , so from eqn. (2.12)  $NSF$  will tend to zero.
- Case II: For a noisy signal,  $X_h \gg X_l$  and  $X_{Nh} \asymp X_{Nl}$ , so from eqn. (2.12)  $NSF$  will be high.
- Case III: For a pure signal,  $Nx_h \asymp Nx_l$  and  $Nh \gg Nl$  so from eqn. (2.13)  $NPF$  will tend to zero.
- Case IV: For a noisy signal,  $N_h \asymp N_l$  and  $Nx_h \gg Nx_l$ , so from eqn. (2.13)  $NPF$  will be high.

Again let us consider two histograms shown in Fig.2.12 (e) and (h). Fig.2.17 (a) and (b) represent two histograms at frequency 10mHz and 75% duty cycle and at 120mHz and

75% duty cycle respectively for sensor TGS-822. These two histograms were taken because from the experimental results the histogram given by Fig. 2.12 (e) for 10mHz and 75% duty cycle provided the best suitable results in the statistical noise feature analysis whereas the histogram given by Fig. 2.12 (h) for 120mHz and 75% duty cycle yielded more noise than at other frequencies and duty cycles.

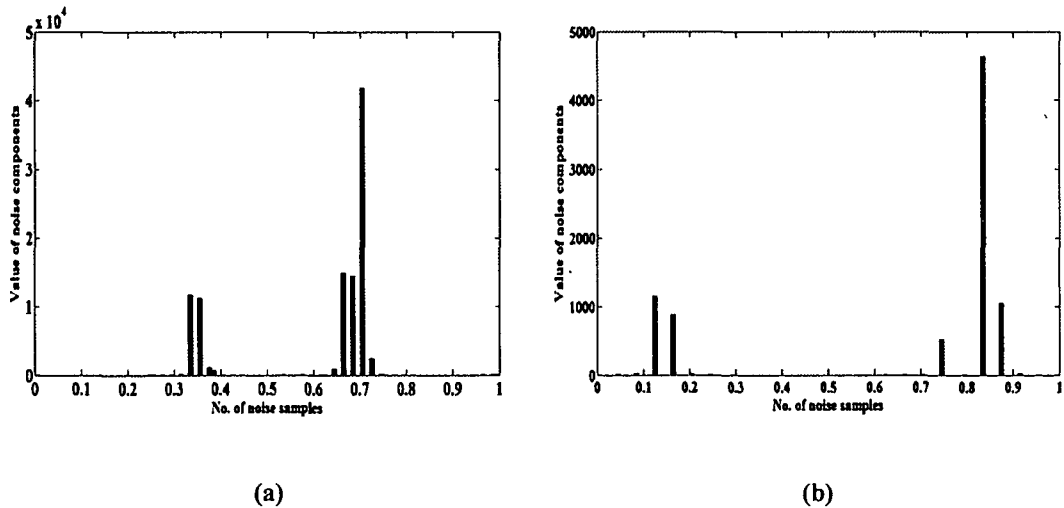


**Fig. 2.17.** Histogram of sensor TGS-822 (a) at frequency 10mHz and 75% duty cycle and (b) at frequency 120mHz and 75% duty cycle.

The two ratios NSF and NPF for the two figures are calculated as follows:

For better accuracy we consider a threshold size of histogram as 200 samples and signal value as 0.34 i.e. we discard the values below these threshold levels. The histogram components for Fig. 2.17(a) are-

$$X_h = 0.73; X_l = 0.34; X_{N_h} = 0.71; X_{N_l} = 0.38; N_h = 41850; N_l = 686; N_{X_h} = 3000;$$

$$N_{X_l} = 11000$$

$$\text{Therefore, } \frac{X_h}{X_l} = 2.1; \frac{X_{N_h}}{X_{N_l}} = 1.8; \frac{N_h}{N_l} = 61; \frac{N_{X_h}}{N_{X_l}} = 0.2727$$

$$\text{Hence, } (\text{NSF})_{10\text{mHz}, 75\%} = \frac{X_h/X_l}{X_{N_h}/X_{N_l}} = 1.17$$

$$\text{and } (\text{NPF})_{10\text{mHz}, 75\%} = \frac{N_{X_h}/N_{X_l}}{N_h/N_l} = 0.004$$

The histogram components for Fig. 2.17(b) are-

$$X_h = 0.88; X_l = 0.12; X_{N_h} = 0.84; X_{N_l} = 0.74; N_h = 4633; N_l = 480; N_{X_h} = 1200;$$

$$N_{X_l} = 1300$$

$$\text{Therefore, } \frac{X_h}{X_l} = 7.3; \quad \frac{X_{N_h}}{X_{N_l}} = 1.135; \quad \frac{N_h}{N_l} = 9.652; \quad \frac{N_{X_h}}{N_{X_l}} = 0.923$$

$$\text{Hence, (NSF)}_{120\text{mHz}, 75\%} = \frac{X_h/X_l}{X_{N_h}/X_{N_l}} = 6.43$$

$$\text{and (NPF)}_{120\text{mHz}, 75\%} = \frac{N_{X_h}/N_{X_l}}{N_h/N_l} = 0.095$$

Thus comparing the values of NSF and NPF for both, Fig. 2.17 (a) and 2.17 (b) we find that at 10mHz and 75% duty cycle, the values of NSF and NPF are higher than at 120mHz and 75% duty cycle indicating that the noise spread is high and with high population i.e. signal is less noisy in case of the former. It is also observed that the high spread with more population as given in Fig. 2.17 (b) is noisier than low spread with high population.

Hence, for a particular noise or noisy signal, as the noise level increases, the spread ratios shown in eqns. (2.8), (2.9), (2.10) and (2.11) increases and as a result the NSF of eqn. (2.12) and NPF of eqn. (2.13) increases. Hence these two noise figure terms can be used to indicate the noise level of a signal. The NSF and NPF calculated from eqn. (2.12) and (2.13) respectively are tabulated in Table 2.4 for all the four different frequencies and duty cycles. From Table 2.5 it is observed that the NSF and NPF ratios for all three sensors increase as the pulsed heater voltage frequency is increased. Also for higher duty cycle, the NSF and NPF ratios decrease. This conforms to the results of other statistical features obtained from Table 2.4. It is observed that at low heater pulse frequencies the noise spread and noise population is smaller.

**Table 2.5** Noise Spread Figure and Noise Population Figure variation with pulse frequency and duty cycle (best suitable values are shown in bold).

Sensor	Duty cycle	Pulse Frequency ( mHz)	NSF	NPF
TGS-822	50%	10	2 80	0 0067
		40	4 49	0 0115
		80	5 74	0 125
		120	6 46	2 818
	75%	10	1.17	<b>0.004</b>
		40	1 65	0 026
		80	1 85	0 065
		120	6 43	0 095
TGS-842	50%	10	2 67	0 012
		40	3 12	0 014
		80	3 66	0 0164
		120	4 52	0 032
	75%	10	1.32	<b>0.01</b>
		40	2 59	0 025
		80	2 89	0 03
		120	3 56	0 44
TGS-2611	50%	10	1 315	0 017
		40	1 492	0 019
		80	1 97	0 16
		120	2 04	0 287
	75%	10	1.08	<b>0.011</b>
		40	1 12	0 209
		80	1 4	0 261
		120	1 98	1 313

## 2.4 Frequency analysis:

The frequency spectrum of a time-domain signal is a representation of that signal in the frequency domain which is determined by FFT analysis.

### 2.4.1 Fast Fourier Transform (FFT):

A fast Fourier transform (FFT) is an efficient algorithm for computing the discrete Fourier transform (DFT) and its inverse. Fourier's representation of functions as a

superposition of sines and cosines are common in the analysis of communication signals and systems. The usefulness of Fourier Transform (FT) lies in its ability to analyze a signal in the time domain for its frequency content. The DFT estimates the Fourier Transform of a function from a finite number of its sampled points. The FFT can be used only when the samples are spaced uniformly. When a continuous-time signal such as the sensor response is sampled at a uniform rate, the resulting sample values may be treated as a discrete-time signal and processed using the FFT. The applications of FFT include systems analysis, digital filtering, simulation, power spectrum analysis, communication theory, etc.

For a response sequence  $x$  of length  $n$ , the DFT is a vector  $X$  of length  $n$ , whose elements are defined as:

$$X(k) = \sum_{p=0}^{n-1} x(p) e^{-j2\pi kp/n} \quad (2.14)$$

where  $k=0,1,\dots,n-1$ .

A common use of FFT is to find the frequency components of a signal buried in a noisy time domain signal. It gives the spectrum of the signal. The measurement of noise levels depends on the bandwidth of the measurement. The noise floor of a power spectrum is actually the narrowband noise level in each FFT bin.

#### 2.4.2 Random White Noise Behavior

**White noise** is a random signal with a flat power spectral density containing equal power within a fixed bandwidth at any center frequency as shown in Fig.2.18. It shows equal amount of fluctuations at all frequencies and its fluctuation at any instant of time is independent of the fluctuations at other times.

A noise signal  $x[n]$  is white if it has zero mean;  $E(x[n]) = 0$  for all  $n$ , with  $E(x[n])$  being the expected value of the random variable  $x[n]$ . Further, white noise have unit variance;  $E(x[n]x[n]) = 1$ , for all  $n$ , and lastly it can be said that the noise signal  $x[n]$  is white if it is independent from sample to sample, i.e. not correlated in time;  $E(x[n]x[n - k]) = 0$ , for  $k \neq 0$  and for all  $n$ . The analysis of a white noise signal in the frequency domain poses

several problems such as it is not periodic, has no finite extent and has infinite energy. Power spectral density function can be used to handle such problems.

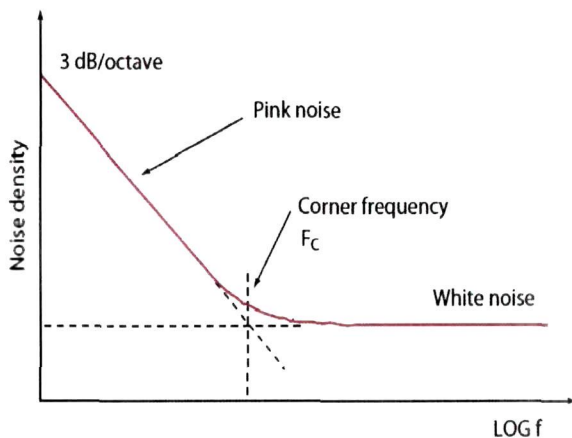


**Fig. 2.18.** White noise power spectral density.

The power spectrum of white noise is homogeneously distributed across the frequencies. Since random signals are non-periodic in nature their spectra varies from time to time and a large number of samples or a long time period is necessary to characterize their average spectral properties. A white noise signal may have Gaussian amplitude distribution or it may have some other distribution i.e. the statistical properties do not determine the shape of the spectrum. The spectra of white noise become flatter with frequency as larger number of samples is used to compute it.

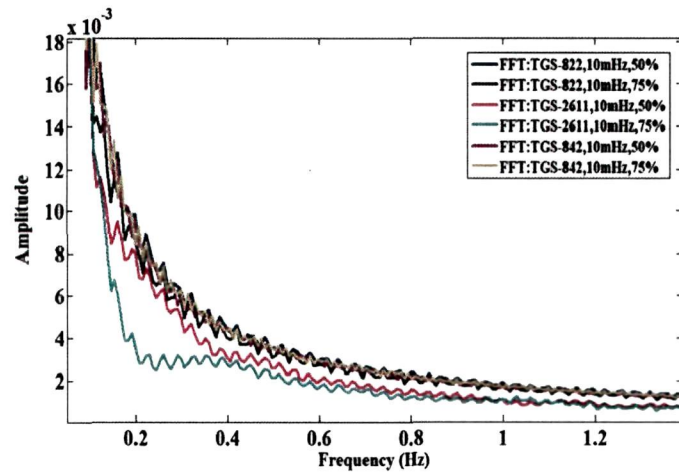
In this study, the frequency spectrum of the sensor signal falls off steadily into the higher frequencies as depicted in Fig.2.18 and the flat part of the noise graph i.e. the noise floor becomes constant over a frequency termed as white noise.

#### 2.4.3 Bandwidth

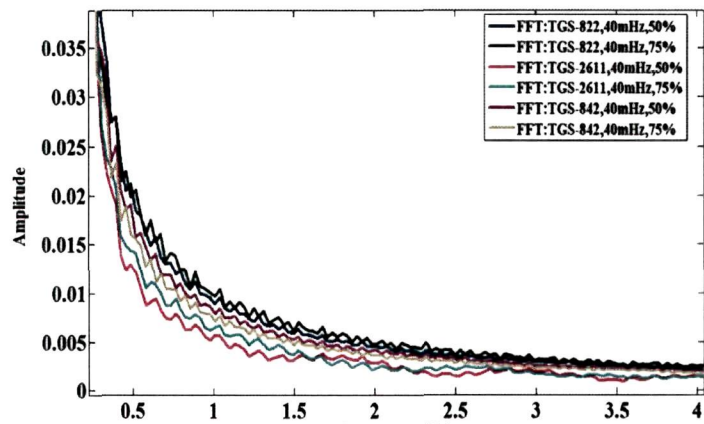
In general, bandwidth is the difference between the upper and lower frequencies in a continuous set of data typically measured in hertz. The characteristic of bandwidth is that a band of a given width can carry the same amount of information, regardless of where that band is located in the frequency spectrum. Most commonly, bandwidth is measured as the 3-dB bandwidth, that is, the frequency range within which the spectral

density is above half its maximum value or the spectral amplitude is more than 70.7% of its maximum.

In this work the noise bandwidth of the sensor response is determined for four different frequencies and two duty cycles of the pulsed heater voltage. FFT was performed for the determination of the bandwidth as tabulated in Table 2.4. Fig. 2.19 shows the FFT of TGS-822, TGS-842 and TGS-2611 at 10 mHz, 40mHz, 80mHz and 120 mHz each at pulsed duty cycles of 50 % and 75 % respectively. The frequency component of noise in case of the sensors TGS-842 and TGS-2611 is smaller at higher frequencies and the noise bandwidth is close to dc as seen from the table.



(a)



(b)

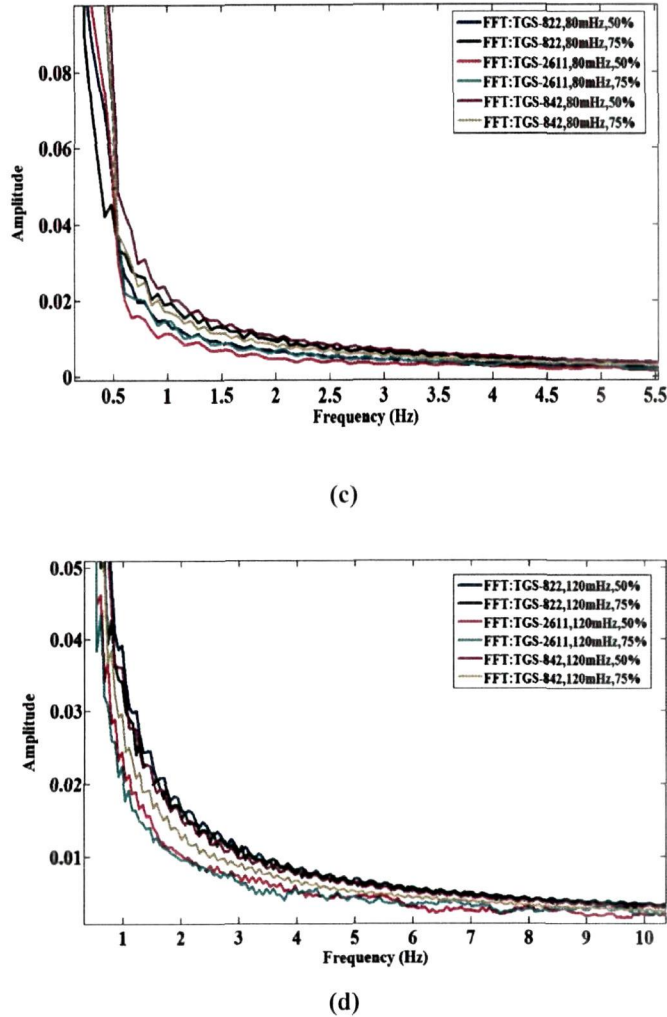


**Fig. 2.19.** The FFT of TGS-822, TGS-2611 and TGS-842 sensor noise signals at 50% and 75% duty cycles for (a) 10mHz , (b) 40mHz , (c) 80mHz and (d) 120mHz.

From the FFT a higher noise bandwidth was observed when pulse frequency was increased. Similarly it is seen that the duty cycle of pulse also contributes to the noise bandwidth with reverse dependency i.e. noise bandwidth decreases as duty cycle increases.

## 2.5 Discussions

In this study, the noise features of MOS gas sensor applying pulse modulated temperature with different frequencies and duty cycles are analyzed. To verify the noise dependency on the frequency and duty cycle of the modulated heater voltage, the PDF, SNR, histogram and FFT of the MOS gas sensor noise was performed. The statistical

analysis reveals that - the noise floor level decreases as the duty cycle of the pulsed modulated heater voltage is increased and pulse frequency is decreased. The same observation is evident for the FFT of the sensor responses that produces higher noise-bandwidth at higher heater pulse frequency however at lower duty cycle. The sensor noise is found to be  $1/f$  or pink and it increases with the increase in pulsed heater voltage frequency and vice-versa. The PDF for the sensor noise signals satisfies the requirement for the noise to be coloured i.e. with non-zero mean. This part of the research deals with the study of noise in the MOS gas sensors without application of gas but under application of pulsed heater temperature. It was observed in this experiment that the characteristics show different behaviour for different patterns of pulsed heater voltage (i.e. heater temperature) with variable frequency and duty cycle.

The noise behavior of the three MOS gas sensors TGS-2611, TGS-822 and TGS-842 was studied with the help of the two newly introduced characteristic figures- NSF and NPF at four different frequencies namely 10mHz, 40mhz, 80mHz and 120mHz and at two different duty cycles namely 50% and 75%. NSF and NPF ratios also conforms to our previous statistical and FFT results i.e. decrease at lower frequency and higher duty cycle. Hence we are able to conclude that the heater pulse frequency and duty cycle considerably influences the noise behavior of the sensor.

The study confirms that the noise immunity of the sensors is more at higher pulse frequency but less at higher duty cycle. This is because a comparatively fast change in temperature produces spurious output signals. Recently, researchers are trying to extract higher degree of features by applying pulsed heater temperature; there must be a compromise between the highest heater pulse frequency and lowest duty cycle to get the best SNR for a particular sensitivity of the sensor.

This analysis facilitates that for improving the classification efficiency of the sensor array, sensor responses can be generated by using a suitable pulse frequency and duty cycle. The method for improvement of classification efficiency by using the best frequency and duty cycle is discussed in the next section. The best frequency and duty cycle for all the three sensors TGS-822, TGS-842 and TGS-2611 is found to be 10mHz and 75% duty cycle.

## **2.6 Gas classification with the best heater pulse frequency using dynamic features:**

In the first part of this research work (*Section 2.3* and *Section 2.4*), the noise characteristics of an E-Nose array consisting of the same MOS gas sensors TGS-822, TGS-842 and TGS-2611 are studied at four different frequencies and two duty cycles for ten gas vapours. This study determined the best suitable heater pulse frequency and duty cycle for a particular sensor which was used as the operating temperature for the second part of the experiment.

In the second part of this study, the dynamic behavior of the MOS gas sensors are studied at these best selected temperatures and duty cycle and the classification of gas is performed using artificial neural network (ANN) to compare the results before and after the frequency selection.

### **2.6.1 Dynamic analysis of MOS gas sensors**

Dynamic behavior of sensor is the criterion on the basis of which the performance of the sensor can be judged. The faster the dynamic response of the sensor the better is the performance of the sensor. Under static conditions, a sensor is fully described by its static sensitivity and signal amplitude, however, when we vary a stimulant say the heater voltage, the sensor response generally does not follow with perfect fidelity. The reason is that both the sensor and its coupling with the source of stimulus cannot always respond instantly. In other words, a sensor may be characterized with a time-dependent characteristic, which is called a *dynamic characteristic*.

### **2.6.2 Effect of pulse modulation frequency on noise behavior**

By operating the MOS gas sensors in dynamic mode and characterizing their transient responses the selectivity of MOS gas sensors can be increased<sup>128</sup>. The dynamic operation of a sensor can be done by – AC operation mode modulation of the gas concentration and modulation of the sensor operating temperature. A periodic waveform is applied to the sensor input in the AC operation mode instead of a fixed DC power supply, while the sensor heater voltage ( $V_H$ ) is kept constant. Gutierrez et al.<sup>129, 130</sup> have found that the peaks appearing in the impedance plots of tin oxide gas sensors in the presence of

reducing gases are a function of the nature of the adsorbed species. Amrani et al.<sup>131</sup> have found that for a single sensor element, characteristic patterns can be found over a very wide frequency range. The modulation of the gas takes place when analyte molecules interact (adsorption/desorption) with the sensor surface. This process consists in the controlled modulation of the gas concentration which produces an output signal containing information on the dynamic adsorption and desorption processes taking place in the sensor surface. Because of this, the transient signals carry information about these processes that are generated when the controlled modulation of a sensor input parameter is performed. The frequency spectrum of these transient signals can be a source of information containing details on the dynamics of the interaction process and have the potential for gas identification. The transient response of gas sensors in gaseous concentration have been performed by many researchers<sup>132-135</sup>. It has been shown that the dynamic sensor response increases the selectivity of a sensor array<sup>101, 136, 137</sup>.

Research has also been conducted combining both effects simultaneously, analyte concentration modulation and working temperature modulation<sup>138</sup>. This process increases the resolving power of metal oxide sensors. Furthermore, its simplicity makes it especially suited for low-cost applications.

Metal Oxide materials such as SnO<sub>2</sub> and ZnO are widely used as sensitive layer for gas sensors in electronic nose. The electronic nose technology with MOS based gas sensors have been widely applied in odour analysis<sup>139-141</sup> as well as in industries focusing on the improvement of performance. Accordingly, the development of gas sensors for the detection of single gases has seen an increasing interest within the research community. Besides such advantages, gas sensors exhibit a series of unpleasant characteristics such as cross-sensitivity, drift and humidity effects, ageing, poisoning etc. Temperature also affects the dynamic characteristics, particularly when they employ viscous damping. A comparatively fast temperature change may cause the sensor to generate a spurious output signal. Feature extraction using both the steady state and dynamic response of the sensor has been widely used for gas sensors applications. In<sup>100-102</sup>, the authors described techniques for extracting and using the steady-state, the slope as well as the transient response information from the sensor's response. In<sup>142</sup>, dynamic signal extraction techniques and optimal array configuration were used to improve the classification performance. In<sup>104</sup> the sensor response curves were determined using six features which

represented the differences of dynamic behaviour of sensors to different sample gases, in phase space. The degree of difference was used to evaluate how much information was extracted from the response curves by the proposed method. In this work it was found that when the adsorption process becomes short, the reacting time i.e. the reaction between the sensor and the sample gets reduced. In<sup>105</sup> research has been carried out on feature extraction on recovery responses which shows that the shape of the recovery curves did not change much with the reaction time. In<sup>106</sup> recognition time and response recovery time of sensors were determined and the feature extraction was done based on these.

In all the research works mentioned above, analysis were performed on the dynamic responses of the gas sensors. Similar to *response time*, *recovery time* etc. *time constant* is also an important parameter that describes the response behaviour of a MOS gas sensor to a particular gas. Fig. 2.20 shows the dynamic characteristics of a sensor response.

In this part of the research work, we have made an analysis on odour classification using time constants of the sensor response as a feature. The time constant,  $\tau$ , is a measure of the sensor's inertia. In analogous electrical systems, it is equal to the product of capacitance and resistance:  $\tau = CR$ . In thermal terms, it is equal to the product of thermal capacity and thermal resistance. In a first-order system, the response is given by,

$$y(t) = y_m(1 - e^{-t/\tau}), \quad (2.15)$$

where  $y_m$  is steady-state output,  $t$  is time. Substituting  $t = \tau$ , we get,

$$\frac{y}{y_m} = 1 - \frac{1}{e} = 0.6321 \quad (2.16)$$

In other words, after an elapse of time equal to one time constant, the response reaches about 63% of its steady-state level. To explain the relation between the dynamic features- slope, response-time and time-constant we consider Fig. 2.21 as shown below:

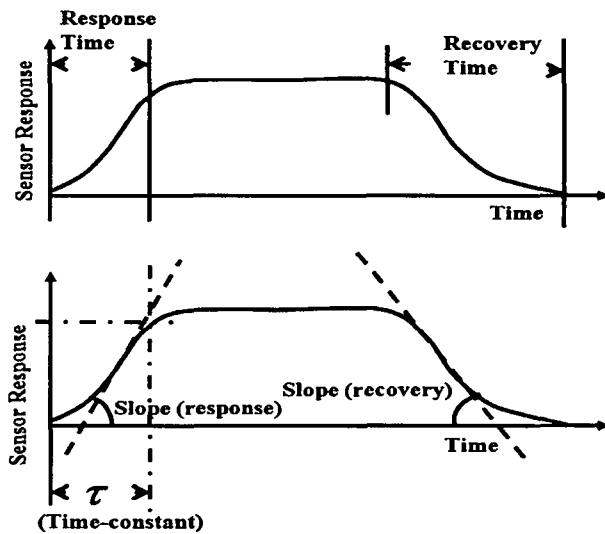


Fig. 2.20: The dynamic features of sensor response.

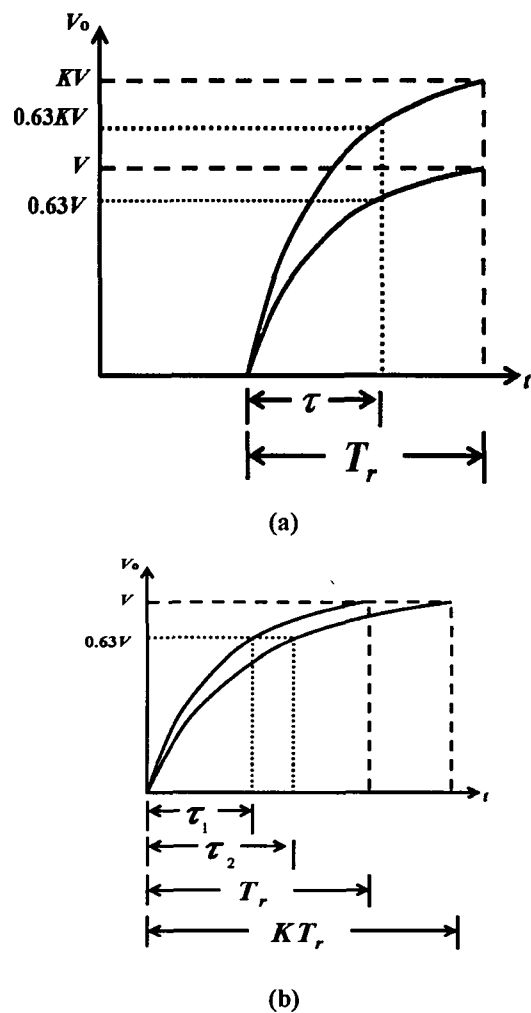


Fig. 2.21: Typical sensor response (a) with constant response time and (b) with constant response voltage.

where  $V$  = Response voltage

$T_r$  = Response time

$K$  = A constant

Now From Fig. 2.21 (a) where the response time  $T_r$  is same but response voltages are different, the slope and time-constant can be written as-

$$\text{Slope} = \frac{V}{T_r} \quad (\text{for response voltage } V) \quad (2.17a)$$

$$\text{and} \quad \text{Slope} = \frac{KV}{T_r} \quad (\text{for response voltage } KV) \quad (2.17b)$$

Time- constant ,

$$\tau = \frac{0.63V}{T_r} = \frac{0.63V}{V} T_r = 0.63T_r \quad (\text{for response voltage } V) \quad (2.17c)$$

$$\text{and} \quad \tau = \frac{0.63KV}{T_r} = \frac{0.63KV}{KV} T_r = 0.63T_r \quad (\text{for response voltage } KV) \quad (2.17d)$$

Similarly from Fig. 2.21 (b) where the response time  $T_r$  is different but response voltages are same, the slope and time-constant can be given as-

$$\text{Slope} = \frac{V}{T_r} \quad (\text{for response time } T_r) \quad (2.18a)$$

$$\text{and} \quad \text{Slope} = \frac{V}{KT_r} \quad (\text{for response time } K T_r) \quad (2.18b)$$

Time-constant,

$$\tau_1 = \frac{0.63V}{T_r} = \frac{0.63V}{V} T_r = 0.63T_r \quad (\text{for response time } T_r) \quad (2.18c)$$

$$\text{and} \quad \tau_2 = \frac{0.63V}{V} = \frac{0.63KV}{V} KT_r = 0.63KT_r \quad (\text{for response time } K T_r) \quad (2.18d)$$

Case I: When the response time is same but response voltages are different, the time-constant is same as given by eqn. (2.17c) and (2.17d). In such cases, the time-constant cannot be a feature for classification.

**Case II:** When the response time is different but response voltages are same, the time-constant is different although with different slopes as given by eqn. (2.18). In such cases, the time-constants can be used as a feature for classification.

Hence time-constant is an important parameter that can be used as a feature for classification of different gases using MOS gas sensors. In our study we have considered the time-constants for each of the ten sample gases as shown in appendix A2.1. These time constants depend on the dynamic behaviour of the sensor responses. During the adsorption process, the sensor response reaches up to a steady state from which the time constants could be determined.

The technique involves pre-processing and feature extraction and of the sensor response, principal component analysis (PCA) and then classification using ANN. The experimental procedures, data acquisition and analysis, results and discussions are described in this chapter. The time constants vary with different sample gases due to the different gas adsorption and heater thermal behaviour. On exposure to the organic gas, the conductance of the sensing element changes while the response time is dependent on the kind of sample gases. The selectivity of MOS gas sensors is greatly influenced by temperature modulation since the rate of reaction for different volatile compounds and the stability of adsorbed oxygen species are dependent on surface temperature. Since the optimum oxidation temperatures vary from gas to gas, a sensor operated at different temperatures behaves as different sensors. The average power consumed by the sensor with the modulated temperature can also be lowered in comparison to sensors working at a constant temperature.

### 2.6.3 Experimental Procedure

The dynamic analysis of MOS gas sensors (TGS-822, TGS-842, TGS-2611 of Figaro, Japan) was conducted for different pulse modulating temperature in the presence of the gases. The experimental set-up has already been described in *Section 2.1.1*. Two vessels were used as gas sample and room air vessels as shown in Fig.2.2. The sample gas and the clean air flow were directed into the chamber containing the sensors through two pumps, which were connected by teflon pipes. The gases from the sample vessel

containing sample gas and the fresh room air were sampled in a sequence for the pre-defined time duration.

The experiment was conducted on the MOS gas sensors with the application of ten different gas samples- ethylacetate, acetonitrile, ethanol, kerosene, petroleum ether, chloroform, methanol, isopropyl alcohol, acetone and n-hexane. Measurements were performed for 100 complete cycles (response and recovery) and a total of 100 data vectors were obtained for each of the 10 sample gases for the three sensors. The measurement was performed for 10 minutes for response followed by 25 minutes for recovery. The heater voltage was modulated at a frequency of 120mHz and 50% duty cycle and then at 10mHz and 75% duty cycle during the sample measurement cycle. The sensor response to fresh air was used as the baseline response for the experiments. Any variations in the baseline, which may occur due to various volatiles present in the room air, were monitored. It was found in each run of experiment that on application of clean air the sensor baseline settles to a fixed level ensuring absence of any interfering gas. The time constants were determined for each cycle and these time responses were used as the sample vectors for the odour classification. The sample measurements were stored in the data file in LabVIEW for further processing in MATLAB.

In the first part of experiments, the sensor temperature was pulsed at an arbitrary selected frequency of 120mHz and duty cycle of 50% to generate the sensor responses in the presence of the ten gases and then the time constants were determined. The sensors were then operated at the best selected pulse modulated frequency and duty cycle i.e. 10mHz and 75% duty cycle to generate the sensor responses in the presence of the 10 gases. The best selected frequency and duty cycle determination was based on the noise analysis as discussed in *Section 2.5*. The classification of data was performed using ANN. Fig2.22 shows an example of the sensor response in LabVIEW for ethanol and acetonitrile showing different response time.

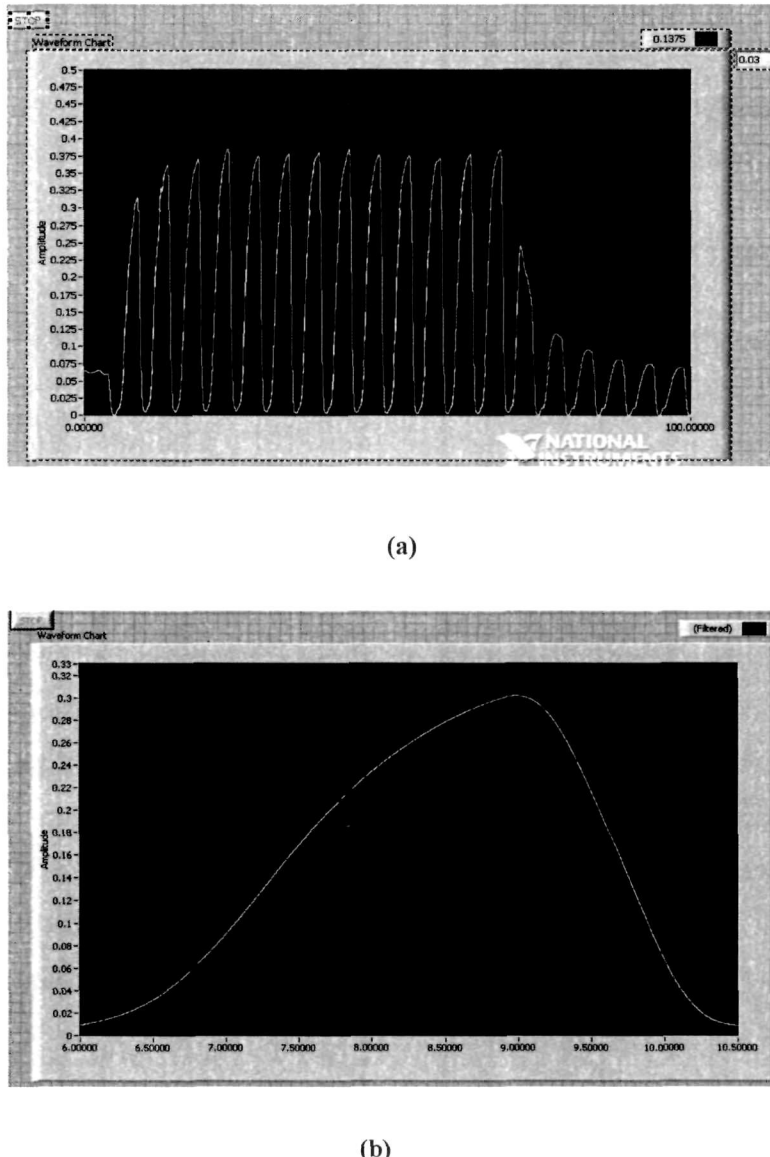


**Fig. 2.22.** The sensor response (TGS-822) in LabVIEW in presence of (a) ethanol and (b) acetonitrile for showing different response time.

#### 2.6.4 Data Acquisition

Data acquisition refers to the process of recording sensor response in a prescribed format at a predefined rate. In this research sufficient amount of data sets were acquired in the long series of experiments. For the sensor data collection, a total time of 175 hrs was required for 100 data vectors from 10 measurement cycles.

## 2.6.5 Data Cluster Analysis

The cluster analysis of sensor data was applied to explore the existence of clusters in feature space within the datasets.

### 2.6.5.1 Feature Extraction Using Principal Component Analysis

PCA is a linear method that has been shown to be effective for the discrimination of sensor data<sup>143</sup>. PCA is a method consisting of expressing the sensor response vectors in terms of linear combination orthogonal vectors. Each principal vector accounts for a certain amount of variance in the data, with a decreasing degree of importance. This was done to reduce the dimensionality of the measurement space, and to extract relevant information for 'pattern recognition'. This dimensionality reduction stage projects the initial feature vector onto a lower dimensional space in order to avoid potential problems associated with high-dimensionality, sparse datasets and so on. Moreover, optimum feature extraction helps in removing a major portion of redundant data, which may be perceived as noise in the signal. The resulting low dimensional feature vector was then used for the classification of the data. It reduces the vector dimension of the dataset and thus makes it possible to identify the most important, or the principal, components. In particular, the first significant component explains the largest percentage of the total variance, the second one, the second largest percentage, and so forth. It is useful for visualizing any patterns existing in the response of a multisensory array data, hence facilitating the detection of odours<sup>144</sup>.

In this analysis, PCA was used to observe the correlation of the sensor data to the classification of the gases. The results of the PCA, using the normalized data vectors at arbitrary frequency of 120mHz and 50% duty cycle is shown in Fig.2.23. The first three principal components were considered for analysis because they accounted for 95.6563% of the variance in the data set.

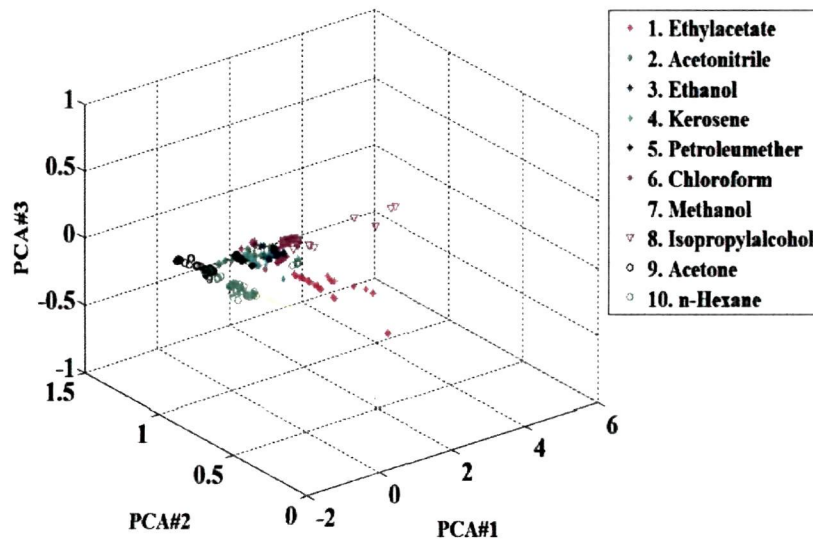


**Fig. 2.23.** PCA plot for the time constants for one gathering cycle of 100 data vectors with heater pulse frequency 120mHz and 50% duty cycle.

The variance and load values for each of 3 principal components (Fig. 2.23) are shown in Table 2.6.

**Table 2.6** The results of PCA for the time constants before selection of frequency and duty cycle.

PC	% Variance	Eigen Values	Principal Components		
			Sensor <sub>1</sub>	Sensor <sub>2</sub>	Sensor <sub>3</sub>
PC <sub>1</sub>	95.6563	0.3143	-0.9826	0.1538	0.1040
PC <sub>2</sub>	3.1172	0.2999	-0.1784	-0.9370	-0.3002
PC <sub>3</sub>	0.2269	0.0152	0.0513	-0.3136	0.9482

It was observed that some samples were easily separated from the rest and form distinct clusters. But some other samples are not easily separable and overlap with other samples. This may be due to the variations of differentiability which are characteristic of the odour of these gas samples. Such results reveal the performance of the gas sensors in finding both the similarity as well as dissimilarity of aroma profiles for the different gas samples.

The results of the PCA, using the normalized data vectors for the selected frequency (10mHz frequency and 75% duty cycle) is shown in Fig.2.24.

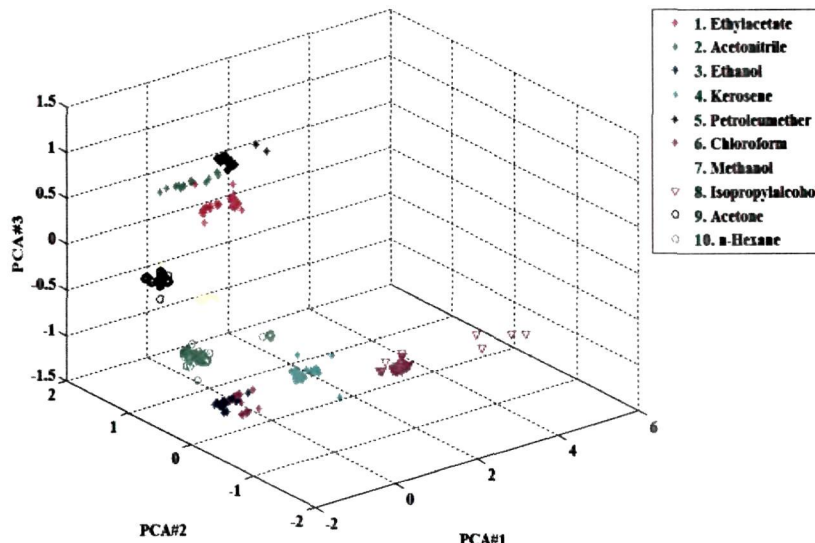


**Fig. 2.24.** PCA plot for the time constants for one cycle of 100 data-vectors with heater frequency 10mHz and 75% duty cycle.

The first three principal components were considered for analysis after selection of frequency and duty cycle because they accounted for 97.4176% of the variance in the data set. The variance and load values for each of 3 principal components (Fig. 2.24) are shown in Table 2.7.

**Table 2.7** The results of PCA for the time constants after selection of frequency and duty cycle.

PC	% Variance	Eigen Values	Principal Components		
			Sensor <sub>1</sub>	Sensor <sub>2</sub>	Sensor <sub>3</sub>
PC <sub>1</sub>	97.4176	0.3761	-0.1023	-0.5411	-0.2133
PC <sub>2</sub>	1.0112	0.2719	-0.0117	-0.6129	0.3422
PC <sub>3</sub>	0.8399	0.0554	0.8210	0.0544	-0.0128

The results of PCA data visualization after selection of frequency and duty cycle indicate that there are ten distinctly separable clusters in the dataset and the sensor data has a better correlation.

### 2.6.5.2 Gas Classification Using Artificial Neural Network

Pattern recognition techniques based on artificial neural networks (ANN) approaches are very widely used for gas sensors<sup>145</sup>. During the learning phase of this approach, sensor response patterns are first trained and presented to the ANN along with respective class affiliations. Performance is then measured as the percentage of odours classified correctly when presenting a test set of new patterns to the ANN. Neural networks learn from examples through iteration, without requiring a priori knowledge of the relationship among variables under investigation. Two different ANN structures namely MLP and RBF were adopted for this stage of data classification. Training of the neural networks was performed with 50% of the whole data set and the rest 50% of the data sets were used for testing the neural network paradigms. A total of 30 data sets of dimensions ( $1 \times 100$ ) for each sensor were formed, thus 15 data sets were used for training and remaining 15 data sets were used to test the performance of the ANN paradigm. The two ANN paradigms were used for the analysis of the comparative results of the sensor data. The structures of the two ANNs are shown in Fig.2.25 (a) and Fig.2.25 (b) and the architecture of the two ANNs used in this experiment is tabulated in Table 2.8.

**Table 2.8** Architecture of the two ANN paradigms (MLP and RBF):

Neural Networks	Architecture
<b>Multi-layer Perceptron (MLP)</b>	3 input neurons, 6 hidden neurons, 10 output neurons, 0.5 adaptive learning rate with momentum 0.42 (one for each sample type).
<b>Radial Basis Function(RBF)</b>	3 input neurons, 10 neurons in the output layer, spread constant 0.8.

#### a) Multi Layer Perceptron (MLP):

An MLP network was programmed in MATLAB environment with an adaptive learning rate of 0.5 and a momentum equal to 0.42. The architecture is shown in Fig.2.24 (a). It has 3 input neurons, from the three sensors, 6 hidden neurons and 10 output neurons chosen for the ten sample gases. The activation function for the neurons in the hidden layers employed is the ‘*logsig*’ function and for the input and output neurons the

activation function is also the ‘*logsig*’ function. The weights were trained with the back propagation algorithm. The network was able to reach a classification rate of 51.9% before the selection of frequency and duty cycle i.e. at 120mHz and 50% duty cycle. After the selection of frequency and duty cycle i.e. at 10mHz and 75% duty cycle the network achieved the classification percentage of 58.21% was obtained.

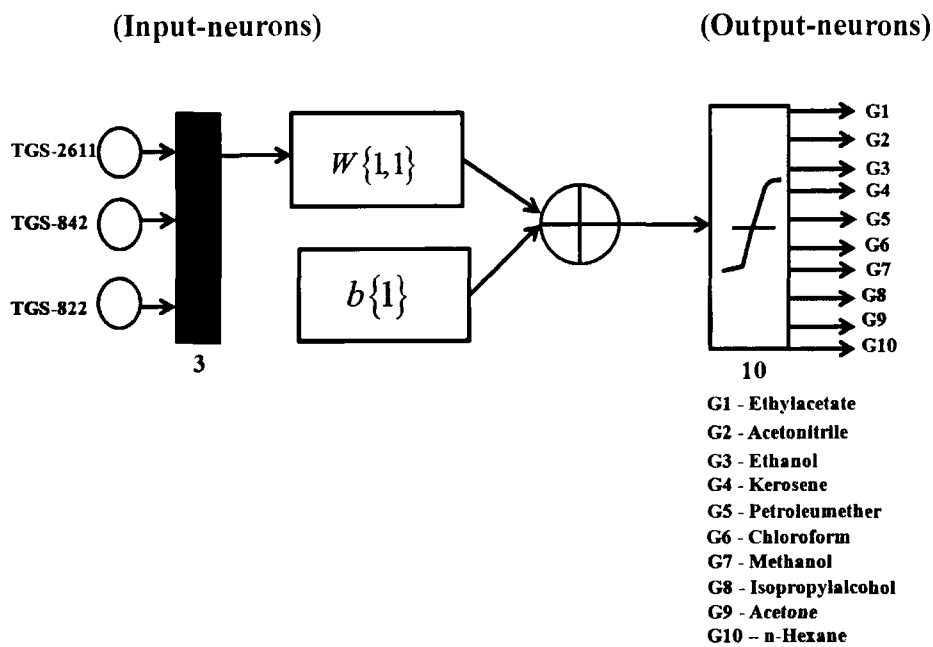


Fig. 2.25 (a). The architecture of MLP for ten sample gases.

The MLP network completed its training for approximately 3000 epochs taking about 1hour training time. Since MLP is poor in adapting the uneven distribution of samples, the classification by MLP was less in comparison to RBF. Table 2.9 shows the training and testing of the data sets on MLP network and its correct classification results for ten sample gases.

**Table 2.9** Training and testing of sensor data on MLP network after the selection of frequency and duty cycle:

Sample Gases	Data vectors for training	Data vectors for testing	% Classification(for 100 data-vectors)
Ethyl Acetate	15(3×300)	15(3×300)	58.21%
Acetonitrile			
Ethanol			
Kerosene			
Petroleum Ether			
Chloroform			
Methanol			
Isopropyl Alcohol			
Acetone			
N-Hexane			

### b) Radial Basis Function (RBF):

The RBF network has been found to be an efficient approach for interpolating scattered data and has been applied in various fields<sup>146</sup>. It has a similar architecture to the MLP, exhibiting fully inter-connected layers. It differs structurally from the MLP in that the hidden layer employs a different type of neuron, called the Radial Basis (RB) neuron. Like MLP, RBF also adopts the supervised learning method, being presented with the input patterns and the associated targets. The RBF network architecture is shown in Fig.2.25 (b). The neurons are added to the network until the sum-squared error (SSE) reduced to a specified error goal which was set as  $10 \times 10^{-6}$ . The spread constant was set at 0.8. The network was able to reach a classification rate of 75.9% before the selection of frequency and duty cycle. After the selection of frequency and duty cycle the network performed the classification of 85.62% was obtained. The training was completed in 100 epochs with a training time of approximately 26 minutes, hence showing better performance and less training time than MLP.

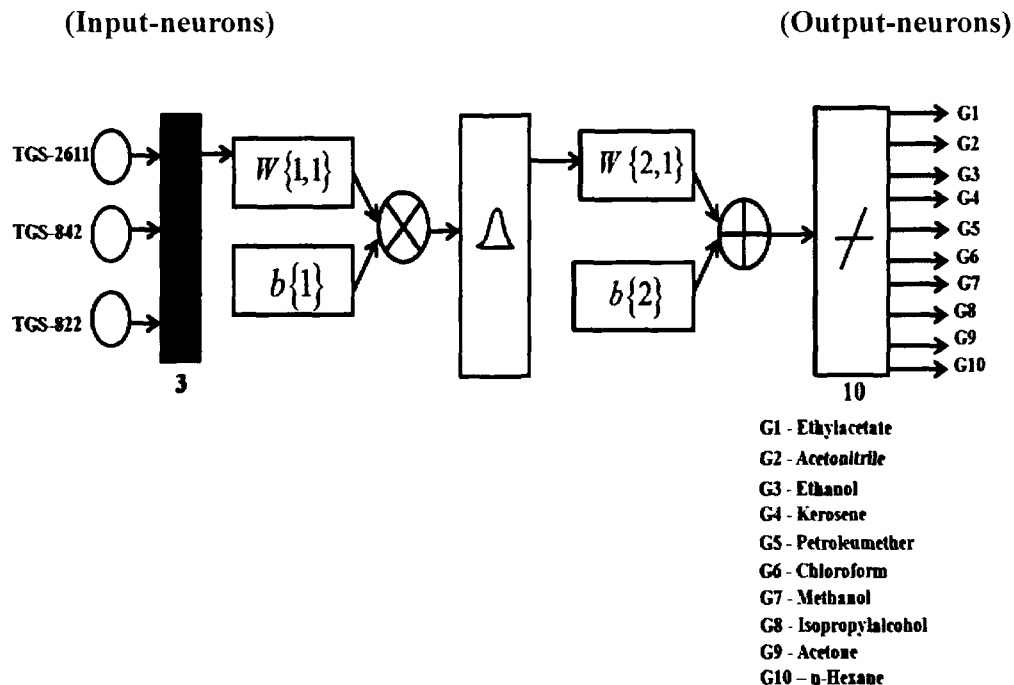


Fig. 2.25 (b). The architecture of RBF for ten sample gases.

#### 2.6.5.3 ANN Performance and Classification Enhancement Results

The training performances of MLP and RBF used in the experiments are shown in Table 2.10. The time required to complete the iterations in case of MLP was more (1 hr approx.) than that for RBF (26 minutes).

**Table 2.10** Training performance of Artificial Neural Network paradigms:

Neural Networks	Training time
Multi-layer Perceptron (MLP)	1 hour
Radial Basis Function(RBF)	26 minutes

The classification of the sensor data (time constants) was performed using the two ANN paradigms. It is seen that the classification is higher in case of RBF than in case of MLP. The classification also improved after selection of the frequency and duty cycle. Table 2.11 shows the classification results of the sensor data for the two ANNs.

From Table 2.11 it is seen that the results of classification improves considerable after the selection of frequency and duty cycle. The classification percentage enhances upto 85.62% using best selected frequency and duty cycle of 10mHz and 75% duty cycle for RBF. Also, the classification with RBF is much higher than that using MLP which improves from 58.21% to 85.62% using the former.

**Table 2.11** Classification results in percentage before and after pulsed frequency selection:

Classification mode	MLP	RBF
Before selection of frequency and duty cycle	51.9%	75.9%
After selection of frequency and duty cycle	58.21 %	85.62 %

## 2.6.6 Results and Discussions

In this part of experiments on the dynamic analysis of MOS gas sensors under pulsed modulated heater voltage, it was found that different sample gases could be classified with the utmost accuracy when the classification of the data was done using best selected temperature i.e. best selected frequency and duty cycle of 10mHz and 75% duty cycle. This frequency was chosen because as per the analysis done in the first part of the experiments, out of the four chosen frequencies of 10mHz, 40mHz, 80mHz and 120mHz and duty cycles of 50% and 75%, the noise was found to be lowest at 10mHz and 75% duty cycle.

It is also concluded that the sensor responses are linearly correlated. A reasonable correlation exists between different sample gases (ten gases used in this case), hence showing that the odour established by PCA is consistent with different sample gases.

The results are tabulated in the Table 2.10. The experiments were performed to classify ten sample gases based on the time constants of the sensors i.e. using time constant as the feature for classification. The classification results of the gases were then compared for data extracted before selection of frequency and duty cycle and for data extracted

after selection of frequency and duty cycle. The classification methods used were PCA, MLP and RBF. From these results (Table 2.7 through Table 2.10), it is evident that the three MOS gas sensors are capable of discriminating the odour of ten sample gases analyzed by the data processing ANN techniques. An accuracy of 85.62% was reached in the classification using RBF network compared with 58.21% using an MLP, thus showing that RBF was much better compared to MLP.

## **2.7 Conclusion:**

This part of the research focuses on the development of a heater pulse frequency and duty cycle selection technique that relies on the fact that frequency and duty cycle of the heater influences the noise behavior of the sensor response and thereby the classification efficiency also. Different data preprocessing and data analyzing techniques were employed. In the first part of experiments-both statistical and frequency spectrum of MOS gas sensor applying pulse modulated temperature with different frequencies and duty cycles are analyzed to study the noise feature. Under statistical analysis-PDF, mean and standard deviation, SNR and histogram was determined. Two new noise characteristic figures- NSF and NPF were introduced at four different frequencies namely 10mHz, 40mhz, 80mHz and 120mHz and at two different duty cycles namely 50% and 75%. It is observed that for a rapid temperature change of sensor temperature, the NSF and NPF ratios increases indicating the rise in the noise level of the signal. Also, it is observed that with the increase in the duty cycle, the NSF and NPF ratios decreases indicating that the level of noise falls off in comparison to the signal level.

Under frequency analysis of sensor data, the FFT analysis of the MOS gas sensor noise is performed to verify the noise dependency on the frequency and duty cycle of the modulated heater voltage by the determination of the noise bandwidth. The study determined the best selected frequency and duty cycle at which the noise was minimum. In the second part of the experiments, the dynamic analysis of the sensor data was done and the discrimination of ten different sample gases was performed using two sets of frequency and duty cycle. At first, the analysis was done using a frequency of 120mHz and 50% duty cycle and then the data was extracted using the best selected frequency and duty cycle of 10mHz and 75% duty cycle. The time constant was used as the feature in this case. LabVIEW (National Instruments) was used to acquire and display the

results. The feature extraction was done using PCA. The PCA results using the normalized data vectors were encouraging, which accounted for upto 98.0004% (Table 2.6) of the variance in case of sensor data before selection and 99.2687% (Table 2.8) of the variance for data after selection of frequency and duty cycle.

Two different ANN structures namely MLP and RBF were adopted for this stage of data classification. Training of the data sets was performed with 50% of the datasets and the rest 50% of the datasets was used for testing the ANN paradigms. The time required for training with MLP was longer than that required for training the network with RBF. Also RBF resulted in a better classification percentage than MLP.

This study is helpful to determine the best suitable heater pulse frequency and duty cycle for a particular sensor. Also from the results of dynamic analysis, it can be concluded that odour classification based on the dynamic responses can be realized using neural networks using gas sensors. Hence, such an approach should have a major role to play in other similar areas of application.

## **2.8 Publication on this chapter**

1. Dutta, N., & Bhuyan, M. Noise Feature Analysis in Pulse Temperature Modulated MOS Gas Sensors, *Sensors and Transducers* **120** (9), 107--118, 2010.
2. Dutta, N., & Bhuyan, M. Statistical Analysis of Noise in MOS Gas Sensor Based Electronic Nose with Pulsed Temperature Modulation, in Computational Vision and Robotics (ICCVR'2010), Bhubaneswar, India, 23-27.
3. Dutta, N., & Bhuyan, M. Dynamic Response Based Odour Classification Using MOS Gas Sensors, in Emerging Applications of Information Technology (EAIT'2011), Kolkata, India, 231-234.